Banner appropriate to article type will appear here in typeset article

Supplementary Information: Three-dimensional soft streaming

Songyuan Cui[1], Yashraj Bhosale[1], and Mattia Gazzola[123]†

[1]Mechanical Sciences and Engineering, University of Illinois at Urbana-Champaign, Urbana, IL 61801, USA

[2]National Center for Supercomputing Applications, University of Illinois at Urbana-Champaign, Urbana, IL 61801, USA

[3]Carl R. Woese Institute for Genomic Biology, University of Illinois at Urbana-Champaign, Urbana, IL 61801, USA

(Received xx; revised xx; accepted xx)

1. Derivation of viscous streaming solution for elastic bodies

Here we present a detailed, step-by-step derivation of the viscous streaming solution in the case of a hyperelastic three-dimensional sphere. The logic of our derivation is the following—we first present the problem setup with the complete set of governing equations and boundary conditions. We then non-dimensionalize them through appropriate scales, introducing the system's key non-dimensional parameters, together with their ranges in typical settings. We perturb the relevant fields (velocity, deformation, pressure) as an asymptotic series of powers of the non-dimensional oscillation amplitude ϵ, to obtain approximations of the flow field solution at different orders. We derive the purely oscillatory solution at zeroth order $\mathcal{O}(1)$, which reduces to a rigid sphere immersed in a fluid governed by the unsteady Stokes equation. We then derive the next order solution at $\mathcal{O}(\epsilon)$ in two steps. First, we obtain the deformation of the elastic solid due to the zeroth order flow in the fluid phase. Next, we use this deformation to derive the necessary boundary condition for the fluid flow, thus incorporating the effect of elasticity into the rectified streaming flow solution.

This section is organized as follows: problem setup, governing equations and boundary conditions are presented in Section 1.1; their non-dimensionalization and key system-defining parameters are discussed in Section 1.2; candidate perturbation series solution and final form of the relevant equations are shown in'Section 1.3; zeroth order (pure oscillatory) solution is derived in Section 1.4; finally, the first order $\mathcal{O}(\epsilon)$ (steady streaming) flow solution including the effects of elasticity are discussed in Section 1.6.

1.1. *Problem setup and governing equations*

We consider the case of a three-dimensional visco-hyperelastic sphere (Fig. 1) of radius a immersed in a viscous fluid, with the fluid oscillating with velocity $V(t) = \epsilon a\omega \cos \omega t$, where ϵ, ω and t represent the non-dimensional amplitude, angular frequency and time, respectively. We 'pin' the sphere's center using a concentric, rigid spherical inclusion of

† Email address for correspondence: mgazzola@illinois.edu

Abstract must not spill onto p.2

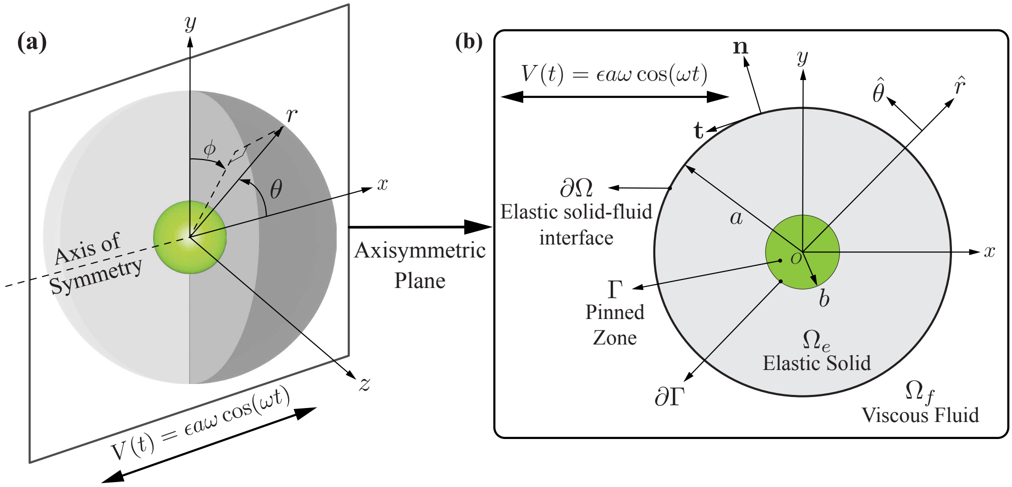

Figure 1: Problem setup. (a) 3D Elastic solid sphere Ω_e of radius a with a rigid inclusion (pinned zone Γ of radius b), immersed in viscous fluid Ω_f. In this study, we deploy the spherical coordinate system where (r, θ, ϕ) are the radial, polar, and azimuthal coordinates. The sphere is exposed to an oscillatory flow with far-field velocity $V(t) = \epsilon a\omega \cos(\omega t)$ in the x direction, along the axis of symmetry. (b) 2D axisymmetric cross-section of the elastic sphere.

radius b, where $b < a$, to kinematically enforce zero strain and velocities near the sphere's center. This pinned zone Γ also serves the purpose of eliminating the trivial solution of the entire sphere vibrating in-sync with the fluid (i.e. $V_{\text{sph}}(t) = \epsilon a\omega \cos \omega t$).

We denote with Ω_e and $\partial\Omega$ the region occupied by the elastic sphere and the boundary between the elastic solid and viscous fluid, respectively. The region occupied by the fluid is represented by Ω_f. The fluid is assumed to be Newtonian, isotropic, and incompressible with density ρ_f and dynamic viscosity μ_f. We further assume that the solid is isotropic and incompressible with constant density ρ_e. The elastic solid is assumed to exhibit viscoelastic Kelvin-Voigt behavior, where stresses are modeled via neo-Hookean hyperelasticity, characteristic of soft biological materials (Bower 2009). Nonetheless, as it will later become apparent, the choice of hyperelastic or viscoelastic model does not affect the general theory presented in this study.

The dynamics in the elastic and fluid phases, in the absence of body forces, is described by the Navier–Stokes (fluid) and the Cauchy (solid) momentum equations

$$
\begin{aligned}
\rho_f \left(\frac{\partial \boldsymbol{v}}{\partial t} + (\boldsymbol{v} \cdot \boldsymbol{\nabla})\boldsymbol{v} \right) &= -\nabla p + \mu_f \boldsymbol{\nabla}^2 \boldsymbol{v}, \quad \boldsymbol{x} \in \Omega_f \\
\rho_e \left(\frac{\partial \boldsymbol{v}}{\partial t} + (\boldsymbol{v} \cdot \boldsymbol{\nabla})\boldsymbol{v} \right) &= -\nabla p + \mu_e \nabla^2 \boldsymbol{v} + \boldsymbol{\nabla} \cdot \boldsymbol{\sigma'}_{he}, \quad \boldsymbol{x} \in \Omega_e
\end{aligned}
\tag{1.1}
$$

where p and $\boldsymbol{v}$ correspond to pressure and velocity fields, respectively. As a convention, the prime symbol $'$ on a tensor $\boldsymbol{A}$ denotes it is deviatoric, i.e. $\boldsymbol{A}' := \boldsymbol{A} - \frac{1}{3} tr(\boldsymbol{A})\boldsymbol{I}$, with $\boldsymbol{I}$ representing the tensor identity and $tr(\cdot)$ representing the trace operator. Thus, $\boldsymbol{\sigma'}_{he}$ corresponds to the deviatoric hyperelastic stress inside the elastic solid, which for a neo-Hookean solid is given by

$$
\boldsymbol{\sigma'}_{he} = G(\boldsymbol{F}\boldsymbol{F}^T)', \tag{1.2}
$$

where $\boldsymbol{F}$ corresponds to a finite strain measure known as the deformation gradient tensor, defined as $\boldsymbol{F} = \partial \boldsymbol{x}/\partial \boldsymbol{X}$. Here $\boldsymbol{X}$ and $\boldsymbol{x}$ correspond to the position of a material point at rest and after deformation, respectively. Alternatively, $\boldsymbol{F}$ can also be written in the form $\boldsymbol{F} = \boldsymbol{I} + \boldsymbol{\nabla u}$, where $\boldsymbol{u}$ is the displacement field defined as $\boldsymbol{u} = \boldsymbol{x} - \boldsymbol{X}$ corresponding to the relative deformation of a material point. Further details regarding derivation of the solid governing equation may be found in supplementary materials, Section §10. In addition, incompressibility translates to the following constraint on the velocity field in the fluid phase

$$\boldsymbol{\nabla} \cdot \boldsymbol{v} = 0, \quad \boldsymbol{x} \in \Omega_f \tag{1.3}$$

and in the solid phase

$$\begin{aligned} \boldsymbol{\nabla} \cdot \boldsymbol{v} &= 0, \quad \boldsymbol{x} \in \Omega_e \\ det(\boldsymbol{F}) &= 1, \quad \boldsymbol{x} \in \Omega_e \end{aligned} \tag{1.4}$$

where $det(\cdot)$ is the determinant operator. We note that $det(\boldsymbol{F}) = 1$ follows from $\boldsymbol{\nabla} \cdot \boldsymbol{v} = 0$ (Jain *et al.* 2019) and it is not an additional constraint.

To close the system of governing equations, we next derive the necessary boundary conditions relative to the pinned zone, interfacial conditions, and far-field conditions. First, the rigid inclusion at the center of the sphere enforces zero velocity and strain fields over its domain Γ

$$\begin{aligned} \boldsymbol{v} &= 0, \quad \boldsymbol{x} \in \Gamma \\ \boldsymbol{u} &= 0, \quad \boldsymbol{x} \in \Gamma. \end{aligned} \tag{1.5}$$

Second, the fluid and elastic solid phases interact exclusively via boundary conditions at the fluid–elastic solid interface. This implies continuity in velocities (no-slip)

$$\boldsymbol{v}_f = \boldsymbol{v}_e, \quad \boldsymbol{x} \in \partial\Omega \tag{1.6}$$

and traction forces (normal and tangential components)

$$\begin{aligned} \boldsymbol{n} \cdot (-p_f \boldsymbol{I} + 2\mu_f \boldsymbol{D}'_f) \cdot \boldsymbol{n} &= \boldsymbol{n} \cdot (-p_e \boldsymbol{I} + 2\mu_e \boldsymbol{D}'_e + G(\boldsymbol{F}\boldsymbol{F}^T)') \cdot \boldsymbol{n}, \qquad \boldsymbol{x} \in \partial\Omega \\ \boldsymbol{n} \cdot (-p_f \boldsymbol{I} + 2\mu_f \boldsymbol{D}'_f) \cdot \boldsymbol{t} &= \boldsymbol{n} \cdot (-p_e \boldsymbol{I} + 2\mu_e \boldsymbol{D}'_e + G(\boldsymbol{F}\boldsymbol{F}^T)') \cdot \boldsymbol{t}, \qquad \boldsymbol{x} \in \partial\Omega \end{aligned} \tag{1.7}$$

where $\boldsymbol{n}$ and $\boldsymbol{t}$ denote the unit outward normal vector and tangent vector at the interface $\partial\Omega$ (Fig. 1). The subscripts e and f refer to elastic and fluid phases respectively. Here, $\boldsymbol{D}'$ is the strain rate tensor $(\boldsymbol{\nabla v} + \boldsymbol{\nabla v}^T)/2$. Finally, the far-field flow velocity must approach the unperturbed oscillatory flow

$$\boldsymbol{v}(|\boldsymbol{x}| \to \infty) = \epsilon a \omega \cos \omega t \; \bar{i}, \quad \boldsymbol{x} \in \Omega_f \tag{1.8}$$

where $\bar{i}$ refers to the oscillation direction. This concludes the definition of our model problem and introduces all governing equations and boundary conditions necessary to its solution.

1.2. *Non-dimensional form and key parameters*

Next, we non-dimensionalize the governing equations and boundary conditions, followed by the identification of the system's key non-dimensional parameters, together with their ranges in typical viscous streaming scenarios. Following the setup of Fig. 1, we choose the characteristic scales of velocity, length and time to be $V = \epsilon a \omega$, $L = a$ and $T = 1/\omega$, respectively. We also define the density ratio as $\alpha = \rho_s/\rho_f$ and the dynamic viscosity ratio as $\beta = \mu_s/\mu_f$. Given that streaming is observed in flow regimes with low to moderate inertia (i.e. large viscous effects), we scale the hydrostatic pressure using viscous stresses, so that the pressure scale is $P = \mu_f V/L$. Non-dimensional relevant quantities and operators can then be expressed as

$$\hat{\boldsymbol{x}} = \frac{\boldsymbol{x}}{a}; \quad \hat{t} = \omega t; \quad \hat{\boldsymbol{v}} = \frac{\boldsymbol{v}}{\epsilon a \omega}; \quad \hat{\boldsymbol{\nabla}} = a\boldsymbol{\nabla}; \quad \hat{p} = \frac{p}{\mu_f \epsilon \omega}; \quad \hat{\boldsymbol{F}} = \boldsymbol{F}; \quad \hat{\boldsymbol{D}}' = \frac{\boldsymbol{D}'}{\epsilon \omega}; \quad \hat{\boldsymbol{n}} = \boldsymbol{n}; \quad \hat{\boldsymbol{t}} = \boldsymbol{t}. \tag{1.9}$$

By substituting the above quantities into Eq. (1.1), we obtain in the fluid phase

$$\left(\frac{\partial \hat{\boldsymbol{v}}}{\partial \hat{t}} + \epsilon(\hat{\boldsymbol{v}} \cdot \hat{\boldsymbol{\nabla}})\hat{\boldsymbol{v}}\right) = -\frac{\mu_f}{\rho_f a^2 \omega}\hat{\nabla}\hat{p} + \frac{\mu_f}{\rho_f a^2 \omega}\hat{\nabla}^2\hat{\boldsymbol{v}}, \quad \hat{\boldsymbol{x}} \in \Omega_f \tag{1.10}$$

and in the solid phase

$$\frac{\epsilon \rho_f a^2 \omega^2}{G}(\alpha)\left(\frac{\partial \hat{\boldsymbol{v}}}{\partial \hat{t}} + \epsilon(\hat{\boldsymbol{v}} \cdot \hat{\boldsymbol{\nabla}})\hat{\boldsymbol{v}}\right) = -\frac{\epsilon \mu_f \omega}{G}\hat{\nabla}\hat{p} + \frac{\epsilon \mu_f \omega}{G}(\beta)\hat{\nabla}^2\hat{\boldsymbol{v}} + \hat{\boldsymbol{\nabla}} \cdot (\hat{\boldsymbol{F}}\hat{\boldsymbol{F}}^T)', \quad \hat{\boldsymbol{x}} \in \Omega_e. \tag{1.11}$$

By introducing the Womersley number $M = a\sqrt{\rho_f \omega / \mu_f}$, which is the inverse of the non-dimensional Stokes layer thickness δ_{AC}/a, and Cauchy number $\mathrm{Cau} = \epsilon \rho_f a^2 \omega^2 / G$, which represents the ratio of inertial to elastic forces, we obtain

$$\left(\frac{\partial \hat{\boldsymbol{v}}}{\partial \hat{t}} + \epsilon(\hat{\boldsymbol{v}} \cdot \hat{\boldsymbol{\nabla}})\hat{\boldsymbol{v}}\right) = -\frac{1}{M^2}\hat{\nabla}\hat{p} + \frac{1}{M^2}\hat{\nabla}^2\hat{\boldsymbol{v}}, \quad \hat{\boldsymbol{x}} \in \Omega_f \tag{1.12}$$

and

$$\mathrm{Cau}(\alpha)\left(\frac{\partial \hat{\boldsymbol{v}}}{\partial \hat{t}} + \epsilon(\hat{\boldsymbol{v}} \cdot \hat{\boldsymbol{\nabla}})\hat{\boldsymbol{v}}\right) = -\frac{\mathrm{Cau}}{M^2}\hat{\nabla}\hat{p} + \frac{\mathrm{Cau}}{M^2}(\beta)\hat{\nabla}^2\hat{\boldsymbol{v}} + \hat{\boldsymbol{\nabla}} \cdot (\hat{\boldsymbol{F}}\hat{\boldsymbol{F}}^T)', \quad \hat{\boldsymbol{x}} \in \Omega_e. \tag{1.13}$$

Similar to the governing equations above, non-dimensionalization transforms Eq. (1.6) and Eq. (1.7) into the following non-dimensional boundary conditions

$$\hat{\boldsymbol{v}}_f = \hat{\boldsymbol{v}}_e \quad \hat{\boldsymbol{x}} \in \partial\Omega \tag{1.14}$$

$$\begin{aligned}
\hat{\boldsymbol{n}} \cdot \left(\frac{\mathrm{Cau}}{M^2}(-\hat{p}_f \boldsymbol{I} + 2\hat{\boldsymbol{D}}'_f)\right) \cdot \hat{\boldsymbol{n}} &= \hat{\boldsymbol{n}} \cdot \left(\frac{\mathrm{Cau}}{M^2}(-\hat{p}_e \boldsymbol{I} + 2(\beta)\hat{\boldsymbol{D}}'_e) + (\hat{\boldsymbol{F}}\hat{\boldsymbol{F}}^T)'\right) \cdot \hat{\boldsymbol{n}}, \qquad \hat{\boldsymbol{x}} \in \partial\Omega \\
\hat{\boldsymbol{n}} \cdot \left(\frac{\mathrm{Cau}}{M^2}(-\hat{p}_f \boldsymbol{I} + 2\hat{\boldsymbol{D}}'_f)\right) \cdot \hat{\boldsymbol{t}} &= \hat{\boldsymbol{n}} \cdot \left(\frac{\mathrm{Cau}}{M^2}(-\hat{p}_e \boldsymbol{I} + 2(\beta)\hat{\boldsymbol{D}}'_e) + (\hat{\boldsymbol{F}}\hat{\boldsymbol{F}}^T)'\right) \cdot \hat{\boldsymbol{t}}, \qquad \hat{\boldsymbol{x}} \in \partial\Omega.
\end{aligned} \tag{1.15}$$

Finally, the incompressibility constraints of Eq. (1.3) and Eq. (1.4), and the pinned zone constraints of Eq. (1.5) remain unchanged, while the far-field condition now reads

$$\hat{\boldsymbol{v}}(|\hat{\boldsymbol{x}}| \to \infty) = \cos t\, \bar{i}, \quad \hat{\boldsymbol{x}} \in \Omega_f. \tag{1.16}$$

We note that the key parameters that define the system behaviour are ϵ, M and Cau. We emphasize that ϵ corresponds to the non-dimensional oscillation amplitude and $\epsilon \ll 1$ for typical viscous streaming applications. The Womersley number M, the inverse of the non-dimensional Stokes layer thickness, is typically $M \geqslant \mathcal{O}(1)$ (Marmottant & Hilgenfeldt 2004; Lutz *et al.* 2006). Accordingly, we assume $\epsilon \ll 1$ and $M = \mathcal{O}(1)$, consistent with assumptions made for 2D soft cylinders (Bhosale *et al.* 2022).

Lastly, the parameter Cau, known as the Cauchy number, represents the ratio of inertial to elastic forces in the system. Here we employ the same assumption for Cau as the 2D soft cylinder case (Bhosale *et al.* 2022), where for a rigid body $\mathrm{Cau} = 0$, and $\mathrm{Cau} > 0$ for an elastic body with $\mathrm{Cau} \ll 1$ implying a weakly elastic body. We note that dealing with $\mathrm{Cau} \geqslant \mathcal{O}(1)$ is mathematically challenging due to the highly non-linear nature of the stress-strain response in hyperelastic materials. Here, to gain theoretical insight, we assume that the sphere is instead weakly elastic Cau $\ll 1$ and in particular that Cau $= \kappa\epsilon$, where $\kappa = \mathcal{O}(1)$. This assumption simplifies the application of asymptotics/perturbation theory, allowing us to investigate the effect of body elasticity on the streaming solution in the limit of $\epsilon \to 0$, thus Cau $\to 0$. This is because the problem dependence is reduced to one small parameter ϵ (i.e. Cau and ϵ are assumed to be equally small). For the less significant parameters density ratio α and viscosity ratio β, we assume $\alpha = \mathcal{O}(1)$ and $\beta = \mathcal{O}(1)$. Nonetheless, these assumptions have negligible influence on the final streaming flow solution, as it shall become clear in the following analysis.

1.3. *Perturbation series approach*

Given the above assumptions and limits, we perturb all relevant fields (velocity, pressure, deformation and interface location) as an asymptotic series with powers of ϵ as gauge functions, valid in the limit $\epsilon \to 0$ and Cau $\to 0$. We henceforth drop the use of $[\hat{\cdot}]$ to simplify notations, thus assuming all quantities to be non-dimensional.

With increasing powers of ϵ, we obtain higher order correction terms in the approximate solution, approaching the true problem solution in the limit $\epsilon \to 0$ and Cau $\to 0$. In this work, we aim to derive the solution at least to first order $\mathcal{O}(\epsilon)$, where streaming is known to emerge in the rigid body case. We perturb all relevant quantities to $\mathcal{O}(\epsilon)$ as shown below

$$\begin{aligned}
\boldsymbol{v} &\sim \boldsymbol{v}_0 + \epsilon \boldsymbol{v}_1 + \mathcal{O}\left(\epsilon^2\right) \\
\boldsymbol{u} &\sim \boldsymbol{u}_0 + \epsilon \boldsymbol{u}_1 + \mathcal{O}\left(\epsilon^2\right) \\
\boldsymbol{n} &\sim \boldsymbol{n}_0 + \epsilon \boldsymbol{n}_1 + \mathcal{O}\left(\epsilon^2\right) \\
\boldsymbol{t} &\sim \boldsymbol{t}_0 + \epsilon \boldsymbol{t}_1 + \mathcal{O}\left(\epsilon^2\right) \\
p &\sim p_0 + \epsilon p_1 + \mathcal{O}\left(\epsilon^2\right) \\
\partial\Omega &\sim \partial\Omega_0 + \epsilon \partial\Omega_1 + \mathcal{O}\left(\epsilon^2\right)
\end{aligned} \tag{1.17}$$

where the subscript (0, 1, ...) indicates the order of the solution. *We comment that this may appear different from previous literature examples (*Longuet-Higgins *1998; *Spelman & Lauga *2017) where perturbation series start from the first order $\mathcal{O}(\epsilon)$, namely, $\psi = \epsilon\psi_1 + \epsilon^2\psi_2 + \mathcal{O}(\epsilon^3)$. However, this apparent discrepancy is readily resolved by recalling that our nondimensionalization employs the characteristic velocity $V = \epsilon a \omega$, which stems from our far-field oscillatory boundary condition (Eq. 1.8, identical to previous literature). This characteristic velocity V is of order $\mathcal{O}(\epsilon)$. Thus, upon nondimensionalization, velocity, vector potential, and Stokes streamfunctions drop of one order relative to their dimensional forms. For example, the zeroth order velocity $\boldsymbol{v}_0$ is in fact of order $\mathcal{O}(\epsilon)$, which corresponds to the first order in the alternative expansion approach. Thus, our expansion approach is consistent with classical sphere streaming literature (*Lane *1955; *Wang *1965), as well as mirroring theories for cylinders (*Holtsmark et al. *1954; *Raney et al. *1954; *Bertelsen et al. *1973).*

By substituting the above expansions into Eq. (1.12) and Eq. (1.13) we obtain the following form of the governing equations in the fluid

$$\begin{aligned}
&\left(\frac{\partial(\boldsymbol{v}_0 + \epsilon\boldsymbol{v}_1 + \ldots)}{\partial t} + \epsilon((\boldsymbol{v}_0 + \epsilon\boldsymbol{v}_1 + \ldots)\cdot\boldsymbol{\nabla})(\boldsymbol{v}_0 + \epsilon\boldsymbol{v}_1 + \ldots)\right) \\
&= -\frac{1}{M^2}\nabla(p_0 + \epsilon p_1 + \ldots) + \frac{1}{M^2}\nabla^2(\boldsymbol{v}_0 + \epsilon\boldsymbol{v}_1 + \ldots), \quad \boldsymbol{x} \in \Omega_f
\end{aligned} \tag{1.18}$$

and in the solid phase

$$\kappa\epsilon(\alpha)\left(\frac{\partial(\boldsymbol{v}_0+\epsilon\boldsymbol{v}_1+\ldots)}{\partial t}+\epsilon((\boldsymbol{v}_0+\epsilon\boldsymbol{v}_1+\ldots)\cdot\boldsymbol{\nabla})(\boldsymbol{v}_0+\epsilon\boldsymbol{v}_1+\ldots)\right)$$
$$=-\frac{\kappa\epsilon}{M^2}\nabla(p_0+\epsilon p_1+\ldots)+\frac{\kappa\epsilon}{M^2}(\beta)\nabla^2(\boldsymbol{v}_0+\epsilon\boldsymbol{v}_1+\ldots)$$
$$+\boldsymbol{\nabla}\cdot((\boldsymbol{I}+\boldsymbol{\nabla}\boldsymbol{u}_0+\epsilon\boldsymbol{\nabla}\boldsymbol{u}_1+\ldots)(\boldsymbol{I}+\boldsymbol{\nabla}\boldsymbol{u}_0+\epsilon\boldsymbol{\nabla}\boldsymbol{u}_1+\ldots)^T)',\quad \boldsymbol{x}\in\Omega_e. \tag{1.19}$$

Furthermore, incompressibility in the fluid phase implies

$$\boldsymbol{\nabla}\cdot(\boldsymbol{v}_0+\epsilon\boldsymbol{v}_1+\ldots)=0,\quad \boldsymbol{x}\in\Omega_f \tag{1.20}$$

and in the solid phase

$$\begin{aligned}\boldsymbol{\nabla}\cdot(\boldsymbol{v}_0+\epsilon\boldsymbol{v}_1+\ldots)&=0,\quad \boldsymbol{x}\in\Omega_e\\ det(\boldsymbol{I}+\boldsymbol{\nabla}\boldsymbol{u}_0+\epsilon\boldsymbol{\nabla}\boldsymbol{u}_1+\ldots)&=1,\quad \boldsymbol{x}\in\Omega_e.\end{aligned} \tag{1.21}$$

For the boundary conditions, constraints induced by the pinned zone (Eq. (1.5)) read

$$\begin{aligned}(\boldsymbol{v}_0+\epsilon\boldsymbol{v}_1+\ldots)&=0,\quad \boldsymbol{x}\in\Gamma\\ (\boldsymbol{u}_0+\epsilon\boldsymbol{u}_1+\ldots)&=0,\quad \boldsymbol{x}\in\Gamma.\end{aligned} \tag{1.22}$$

Interfacial boundary conditions Eq. (1.14) and Eq. (1.15) follow as

$$(\boldsymbol{v}_{f,0}+\epsilon\boldsymbol{v}_{f,1}+\ldots)=(\boldsymbol{v}_{e,0}+\epsilon\boldsymbol{v}_{e,1}+\ldots)\quad \boldsymbol{x}\in\partial\Omega \tag{1.23}$$

$$(\boldsymbol{n}_0+\epsilon\boldsymbol{n}_1+\ldots)\cdot\left(\frac{\epsilon\kappa}{M^2}(-(p_{f,0}+\epsilon p_{f,1}+\ldots)\boldsymbol{I}+2(\boldsymbol{D}'_{f,0}+\epsilon\boldsymbol{D}'_{f,1}+\ldots))\right)\cdot(\boldsymbol{n}_0+\epsilon\boldsymbol{n}_1+\ldots)$$
$$=(\boldsymbol{n}_0+\epsilon\boldsymbol{n}_1+\ldots)\cdot\left(\frac{\epsilon\kappa}{M^2}(-(p_{e,0}+\epsilon p_{e,1}+\ldots)\boldsymbol{I}+2(\beta)(\boldsymbol{D}'_{e,0}+\epsilon\boldsymbol{D}'_{e,1}+\ldots))\right.$$
$$\left.+((\boldsymbol{I}+\boldsymbol{\nabla}\boldsymbol{u}_0+\epsilon\boldsymbol{\nabla}\boldsymbol{u}_1+\ldots)(\boldsymbol{I}+\boldsymbol{\nabla}\boldsymbol{u}_0+\epsilon\boldsymbol{\nabla}\boldsymbol{u}_1+\ldots)^T)'\right)\cdot(\boldsymbol{n}_0+\epsilon\boldsymbol{n}_1+\ldots)\ \ \boldsymbol{x}\in\partial\Omega \tag{1.24}$$

$$(\boldsymbol{n}_0+\epsilon\boldsymbol{n}_1+\ldots)\cdot\left(\frac{\epsilon\kappa}{M^2}(-(p_{f,0}+\epsilon p_{f,1}+\ldots)\boldsymbol{I}+2(\boldsymbol{D}'_{f,0}+\epsilon\boldsymbol{D}'_{f,1}+\ldots))\right)\cdot(\boldsymbol{t}_0+\epsilon\boldsymbol{t}_1+\ldots)$$
$$=(\boldsymbol{n}_0+\epsilon\boldsymbol{n}_1+\ldots)\cdot\left(\frac{\epsilon\kappa}{M^2}(-(p_{e,0}+\epsilon p_{e,1}+\ldots)\boldsymbol{I}+2(\beta)(\boldsymbol{D}'_{e,0}+\epsilon\boldsymbol{D}'_{e,1}+\ldots))\right.$$
$$\left.+((\boldsymbol{I}+\boldsymbol{\nabla}\boldsymbol{u}_0+\epsilon\boldsymbol{\nabla}\boldsymbol{u}_1+\ldots)(\boldsymbol{I}+\boldsymbol{\nabla}\boldsymbol{u}_0+\epsilon\boldsymbol{\nabla}\boldsymbol{u}_1+\ldots)^T)'\right)\cdot(\boldsymbol{t}_0+\epsilon\boldsymbol{t}_1+\ldots)\ \ \boldsymbol{x}\in\partial\Omega. \tag{1.25}$$

Finally, the far-field condition reads

$$(\boldsymbol{v}_0+\epsilon\boldsymbol{v}_1+\ldots)(|\boldsymbol{x}|\to\infty)=\cos t\,\bar{i},\quad \boldsymbol{x}\in\Omega_f. \tag{1.26}$$

Before proceeding, we briefly describe the key steps we will follow to derive the flow field solutions at different orders. Given the pinned zone constraints and governing equations in the solid phase, we first derive the solution for the deformation of the elastic body. From this we compute the motion of the solid–fluid interface. This, in turn, provides us with the appropriate boundary conditions to solve the governing equations in the fluid phase.

1.4. *Zeroth order $\mathcal{O}(1)$ governing equations and boundary conditions*

We begin with the derivation of the zeroth order $\mathcal{O}(1)$ solution. Zeroth order equations are obtained by recovering the $\mathcal{O}(1)$ terms from the governing equations Eqs. (1.18) and (1.19) and boundary conditions Eqs. (1.23) to (1.26). Alternatively, the zeroth order equations can be obtained by setting $\epsilon = 0$. First, the fluid phase governing equations Eqs. (1.18) and (1.20) reduce to the incompressible unsteady Stokes equations

$$M^2 \frac{\partial \boldsymbol{v}_0}{\partial t} = -\nabla p_0 + \nabla^2 \boldsymbol{v}_0, \quad \boldsymbol{\nabla} \cdot \boldsymbol{v}_0 = 0, \quad \boldsymbol{x} \in \Omega_f \tag{1.27}$$

while in the elastic solid phase, the governing equations Eqs. (1.19) and (1.21) reduce to

$$\boldsymbol{\nabla} \cdot ((\boldsymbol{I} + \boldsymbol{\nabla} \boldsymbol{u}_0)(\boldsymbol{I} + \boldsymbol{\nabla} \boldsymbol{u}_0)^T)' = 0, \quad \boldsymbol{\nabla} \cdot \boldsymbol{v}_0 = 0, \quad \boldsymbol{x} \in \Omega_e. \tag{1.28}$$

To solve the above equations, we start from the pinned zone constraints of Eq. (1.22), which reduce to

$$\begin{aligned} \boldsymbol{v}_0 &= 0, \quad \boldsymbol{x} \in \Gamma \\ \boldsymbol{u}_0 &= 0, \quad \boldsymbol{x} \in \Gamma. \end{aligned} \tag{1.29}$$

Since Cau = 0 (implied by Cau = $\kappa\epsilon$) the elastic solid is effectively rigid at zeroth order so that the direct solution of Eq. (1.28), with the constraints of Eq. (1.29), corresponds to the fixed rigid sphere

$$\begin{aligned} \boldsymbol{v}_0 = 0, \quad \boldsymbol{u}_0 = 0, \quad \boldsymbol{x} \in \partial\Omega_0 \\ \partial\Omega_0 := r = 1 \end{aligned} \tag{1.30}$$

where $\partial\Omega_0$ is the boundary at the non-dimensional radius $r = 1$. Because of the no-slip boundary condition for the velocity field, and continuity in pressure fields (Angot *et al.* (1999)), we have

$$\begin{aligned} \boldsymbol{v}_{f,0} &= 0, & \boldsymbol{x} \in \partial\Omega_0 \\ p_{f,0} &= p_{e,0}, & \boldsymbol{x} \in \partial\Omega_0 \end{aligned} \tag{1.31}$$

while the far-field condition of Eq. (1.26) reads

$$\boldsymbol{v}_0(|\boldsymbol{x}| \to \infty) = \cos t \; \bar{i}, \quad \boldsymbol{x} \in \Omega_f. \tag{1.32}$$

1.5. *Zeroth order $O(1)$ solution in spherical coordinates*

To solve the above system of equations, we introduce the geometrically convenient spherical coordinate system (r, θ, ϕ), with r being the radial coordinate, θ the angular coordinate, and ϕ the azimuthal coordinate. The origin of the coordinate system is set to be at the center of the sphere, and $\bar{i}$ corresponds to the line of oscillation $\theta = 0$. The no-slip boundary condition Eq. (1.31) and the far-field condition Eq. (1.32) can be written as

$$\begin{aligned} v_{0,r}|_{r=1} &= 0 \\ v_{0,\theta}|_{r=1} &= 0 \\ v_{0,\phi}|_{r=1} &= 0 \\ v_{0,r}|_{r\to\infty} &= \cos\theta \; \cos t \\ v_{0,\theta}|_{r\to\infty} &= -\sin\theta \; \cos t \\ v_{0,\phi}|_{r\to\infty} &= 0. \end{aligned} \tag{1.33}$$

We next drive the zeroth order solution using the vector potential $\boldsymbol{\varphi}_0 = \varphi_0 \hat{\phi}$ form of Eq. (1.27)

$$M^2 \frac{\partial \boldsymbol{\nabla}^2 \boldsymbol{\varphi}_0}{\partial t} = \boldsymbol{\nabla}^4 \boldsymbol{\varphi}_0, \quad r \geqslant 1 \tag{1.34}$$

where $\boldsymbol{v} = \boldsymbol{\nabla} \times \boldsymbol{\varphi} = \boldsymbol{\nabla} \times \varphi \hat{\boldsymbol{\phi}}$, and $\hat{\boldsymbol{\phi}}$ is the unit vector in the azimuthal direction. The solution of the above equation was first derived by Lane (1955) and can be written as

$$\varphi_0 = -\frac{\sin\theta}{4}\left(3\frac{h_1(mr)}{mh_0(m)} - r - \frac{h_2(m)}{r^2 h_0(m)}\right)e^{-it} + c.c., \quad r \geqslant 1 \tag{1.35}$$

where $i = \sqrt{-1}$ and $m = \sqrt{i}M = (1+i)M/\sqrt{2}$, h_n is the n^{th} order spherical Hankel function of the first kind, and $c.c.$ refers to the complex conjugate. By taking the curl of the zeroth-order vector potential, the velocity field $\boldsymbol{v}_0$ is derived as

$$\begin{aligned} v_{0,r} &= \frac{1}{r\sin\theta}\frac{\partial(\varphi_0\sin\theta)}{\partial\theta} \\ &= -\frac{\cos\theta}{2}\left(3\frac{h_1(mr)}{mh_0(m)r} - 1 - \frac{h_2(m)}{r^3 h_0(m)}\right)e^{-it} + c.c \qquad r \geqslant 1 \\ v_{0,\theta} &= -\frac{1}{r}\frac{\partial(r\varphi_0)}{\partial r} \\ &= -\frac{\sin\theta}{4}\left(3\frac{h_1(mr)}{mh_0(m)r} - 3\frac{h_0(mr)}{h_0(m)} + 2 - \frac{h_2(m)}{r^3 h_0(m)}\right)e^{-it} + c.c. \quad r \geqslant 1 \end{aligned} \tag{1.36}$$

where we have used the recurrent identity

$$h_n'(z) = h_{n-1}(z) - \frac{n+1}{z}h_n(z)$$

Eq. (1.36) suggests that the zeroth order velocity field $\boldsymbol{v}_0$ in the fluid is purely oscillatory (time-dependent), and hence no steady streaming manifests at $\mathcal{O}(1)$ (Lane 1955). Additionally, no effects of elasticity on the flow field manifest at zeroth order as Cau = 0 . Therefore, we proceed to perturbation series approximation at $\mathcal{O}(\epsilon)$, where elasticity affects the steady streaming solution.

1.6. *First order $\mathcal{O}(\epsilon)$ governing equations and boundary conditions*

We recover the first order governing equations by extracting the $\mathcal{O}(\epsilon)$ terms from Eq. (1.18) and Eq. (1.19). The fluid phase governing equation (Eq. (1.18)) at order $\mathcal{O}(\epsilon)$ is given as

$$M^2\frac{\partial \boldsymbol{v}_1}{\partial t} + M^2(\boldsymbol{v}_0 \cdot \boldsymbol{\nabla})\boldsymbol{v}_0 = -\nabla p_1 + \nabla^2 \boldsymbol{v}_1, \quad \boldsymbol{x} \in \Omega_f \tag{1.37}$$

while in the solid phase Eq. (1.19), we have

$$\kappa(\alpha)\left(\frac{\partial \boldsymbol{v}_0}{\partial t}\right) = -\frac{\kappa}{M^2}\nabla p_0 + \frac{\kappa}{M^2}(\beta)\nabla^2\boldsymbol{v}_0 + \boldsymbol{\nabla}\cdot(\boldsymbol{\nabla}\boldsymbol{u}_1 + (\boldsymbol{\nabla}\boldsymbol{u}_1)^T)', \quad \boldsymbol{x} \in \Omega_e. \tag{1.38}$$

We then substitute Eq. (1.31) into Eq. (1.38) to obtain

$$\kappa\nabla p_0 = M^2\boldsymbol{\nabla}\cdot(\boldsymbol{\nabla}\boldsymbol{u}_1 + (\boldsymbol{\nabla}\boldsymbol{u}_1)^T)', \quad \boldsymbol{x} \in \Omega_e. \tag{1.39}$$

We note in this step the disappearance of the density (α) and viscosity (β) ratios, rendering them insignificant at order $\mathcal{O}(\epsilon)$. To simplify Eq. (1.39), we note that the incompressibility constraint Eq. (1.21) reduces to the following at $\mathcal{O}(\epsilon)$

$$det(\boldsymbol{I} + \epsilon\boldsymbol{\nabla}\boldsymbol{u}_1) = 1, \quad \boldsymbol{x} \in \Omega_e. \tag{1.40}$$

Using the following 3D determinant identity

$$det(\boldsymbol{A}+\boldsymbol{B}) = det(\boldsymbol{A}) + det(\boldsymbol{B}) + det(\boldsymbol{A})\cdot tr(\boldsymbol{A}^{-1}\boldsymbol{B}) + det(\boldsymbol{B})\cdot tr(\boldsymbol{A}\boldsymbol{B}^{-1})$$

with $\boldsymbol{A} = \boldsymbol{I}$, $det(\boldsymbol{A}) = 1$, $\boldsymbol{B} = \epsilon\nabla\boldsymbol{u}_1$, at $O(\epsilon)$ the constraint further reduces to

$$tr(\nabla\boldsymbol{u}_1) = \nabla\cdot\boldsymbol{u}_1 = 0, \quad \boldsymbol{x}\in\Omega_e. \tag{1.41}$$

which suggests incompressibility in elastic solid's displacement field at $O(\epsilon)$. The solid phase governing equation Eq. (1.39) is then simplified into

$$\kappa\nabla p_0 = M^2\nabla^2\boldsymbol{u}_1, \quad \boldsymbol{x}\in\Omega_e. \tag{1.42}$$

The above equation physically represents the zeroth-order fluid flow ($\kappa\nabla p_0$ term) deforming the first-order weakly elastic solid ($\boldsymbol{u}_1$). As pointed out previously, Eq. (1.39) shows how the choice of hyperelastic or viscoelastic model does not affect equations at $O(\epsilon)$ as all nonlinear terms are of higher orders. It represents a linear approximation of the hyperelastic model (Eq. (1.2)), where higher order non-linear terms in the stress strain response drop out.

To solve the governing equations $O(\epsilon)$ Eq. (1.37) and Eq. (1.42), we consider the boundary conditions starting from the pinned zone constraints of Eq. (1.22), which at $O(\epsilon)$ read

$$\boldsymbol{v}_1 = 0, \quad \boldsymbol{u}_1 = 0, \quad \boldsymbol{x}\in\Gamma. \tag{1.43}$$

Next, we consider the solid–fluid interfacial stress boundary conditions of Eq. (1.24) and Eq. (1.25), which when evaluated at $O(\epsilon)$ accurate interface $\partial\Omega_0 + \epsilon\partial\Omega_1$, with substitution of Eq. (1.31) give

$$
\begin{aligned}
\boldsymbol{n}\cdot\left(\frac{\mathrm{Cau}}{M^2}(-p_f\boldsymbol{I}+2\boldsymbol{D}'_f)\right)\cdot\boldsymbol{n}\Big|_{\partial\Omega} &= \epsilon\boldsymbol{n}_0\cdot\left(\frac{\kappa}{M^2}(-p_{f,0}\boldsymbol{I}+2\boldsymbol{D}'_{f,0})\right)\cdot\boldsymbol{n}_0\Big|_{\partial\Omega_0+\epsilon\partial\Omega_1}+\mathcal{O}\left(\epsilon^2\right)\\
&= \epsilon\boldsymbol{n}_0\cdot\left(\frac{\kappa}{M^2}(-p_{f,0}\boldsymbol{I}+2\boldsymbol{D}'_{f,0})\right)\cdot\boldsymbol{n}_0\Big|_{\partial\Omega_0}+\mathcal{O}\left(\epsilon^2\right)\\
&= \boldsymbol{n}\cdot\left(\frac{\mathrm{Cau}}{M^2}(-p_e\boldsymbol{I}+2(\beta)\boldsymbol{D}'_e)+(\boldsymbol{F}\boldsymbol{F}^T)'\right)\cdot\boldsymbol{n}\Big|_{\partial\Omega}\\
&= \epsilon\boldsymbol{n}_0\cdot\left(\frac{\kappa}{M^2}(-p_{e,0}\boldsymbol{I}+2(\beta)\boldsymbol{D}'_{e,0})+(\nabla\boldsymbol{u}_1+(\nabla\boldsymbol{u}_1)^T)'\right)\cdot\boldsymbol{n}_0\Big|_{\partial\Omega_0+\epsilon\partial\Omega_1}\\
&+\mathcal{O}\left(\epsilon^2\right)\\
&= \epsilon\boldsymbol{n}_0\cdot\left(\frac{\kappa}{M^2}(-p_{e,0}\boldsymbol{I}+2(\beta)\boldsymbol{D}'_{e,0})+(\nabla\boldsymbol{u}_1+(\nabla\boldsymbol{u}_1)^T)'\right)\cdot\boldsymbol{n}_0\Big|_{\partial\Omega_0}\\
&+\mathcal{O}\left(\epsilon^2\right)\\
\boldsymbol{n}\cdot\left(\frac{\mathrm{Cau}}{M^2}(-p_f\boldsymbol{I}+2\boldsymbol{D}'_f)\right)\cdot\boldsymbol{t}\Big|_{\partial\Omega} &= \epsilon\boldsymbol{n}_0\cdot\left(\frac{\kappa}{M^2}(-p_{f,0}\boldsymbol{I}+2\boldsymbol{D}'_{f,0})\right)\cdot\boldsymbol{t}_0\Big|_{\partial\Omega_0+\epsilon\partial\Omega_1}+\mathcal{O}\left(\epsilon^2\right)\\
&= \epsilon\boldsymbol{n}_0\cdot\left(\frac{\kappa}{M^2}(-p_{f,0}\boldsymbol{I}+2\boldsymbol{D}'_{f,0})\right)\cdot\boldsymbol{t}_0\Big|_{\partial\Omega_0}+\mathcal{O}\left(\epsilon^2\right)\\
&= \boldsymbol{n}\cdot\left(\frac{\mathrm{Cau}}{M^2}(-p_e\boldsymbol{I}+2(\beta)\boldsymbol{D}'_e)+(\boldsymbol{F}\boldsymbol{F}^T)'\right)\cdot\boldsymbol{t}\Big|_{\partial\Omega}\\
&= \epsilon\boldsymbol{n}_0\cdot\left(\frac{\kappa}{M^2}(-p_{e,0}\boldsymbol{I}+2(\beta)\boldsymbol{D}'_{e,0})+(\nabla\boldsymbol{u}_1+(\nabla\boldsymbol{u}_1)^T)'\right)\cdot\boldsymbol{t}_0\Big|_{\partial\Omega_0+\epsilon\partial\Omega_1}\\
&+\mathcal{O}\left(\epsilon^2\right)\\
&= \epsilon\boldsymbol{n}_0\cdot\left(\frac{\kappa}{M^2}(-p_{e,0}\boldsymbol{I}+2(\beta)\boldsymbol{D}'_{e,0})+(\nabla\boldsymbol{u}_1+(\nabla\boldsymbol{u}_1)^T)'\right)\cdot\boldsymbol{t}_0\Big|_{\partial\Omega_0}\\
&+\mathcal{O}\left(\epsilon^2\right).
\end{aligned}
\tag{1.44}
$$

Retention of $\mathcal{O}(\epsilon)$ terms in Eq. (1.44) gives us

$$
\begin{aligned}
\boldsymbol{n}_0\cdot\left(\frac{\kappa}{M^2}(-p_{f,0}\boldsymbol{I}+2\boldsymbol{D}'_{f,0})\right)\cdot\boldsymbol{n}_0 &= \boldsymbol{n}_0\cdot\left(\frac{\kappa}{M^2}(-p_{e,0}\boldsymbol{I}+2(\beta)\boldsymbol{D}'_{e,0})+(\nabla\boldsymbol{u}_1+(\nabla\boldsymbol{u}_1)^T)'\right)\cdot\boldsymbol{n}_0\\
\boldsymbol{n}_0\cdot\left(\frac{\kappa}{M^2}(-p_{f,0}\boldsymbol{I}+2\boldsymbol{D}'_{f,0})\right)\cdot\boldsymbol{t}_0 &= \boldsymbol{n}_0\cdot\left(\frac{\kappa}{M^2}(-p_{e,0}\boldsymbol{I}+2(\beta)\boldsymbol{D}'_{e,0})+(\nabla\boldsymbol{u}_1+(\nabla\boldsymbol{u}_1)^T)'\right)\cdot\boldsymbol{t}_0,\\
&\boldsymbol{x}\in\partial\Omega_0.
\end{aligned}
\tag{1.45}
$$

Here, $\boldsymbol{n}_0$ and $\boldsymbol{t}_0$ refer to the normal and tangent vectors at the zeroth order at the rigid body interface $\partial\Omega_0$. These conditions (Eq. 1.45) can be simplified using Eqs. (1.30) and (1.31) to obtain

$$
\begin{aligned}
\boldsymbol{n}_0\cdot\left(2\boldsymbol{D}'_{f,0}\right)\cdot\boldsymbol{n}_0 &= \boldsymbol{n}_0\cdot\left(\frac{M^2}{\kappa}(\nabla\boldsymbol{u}_1+(\nabla\boldsymbol{u}_1)^T)'\right)\cdot\boldsymbol{n}_0, && \boldsymbol{x}\in\partial\Omega_0\\
\boldsymbol{n}_0\cdot\left(2\boldsymbol{D}'_{f,0}\right)\cdot\boldsymbol{t}_0 &= \boldsymbol{n}_0\cdot\left(\frac{M^2}{\kappa}(\nabla\boldsymbol{u}_1+(\nabla\boldsymbol{u}_1)^T)'\right)\cdot\boldsymbol{t}_0, && \boldsymbol{x}\in\partial\Omega_0.
\end{aligned}
\tag{1.46}
$$

1.7. *First order $O(\epsilon)$ solution in spherical coordinates*

With $O(\epsilon)$ governing equations and boundary conditions obtained, we proceed as before to derive their analytical solution. We start by deriving an expression for the displacement field $\boldsymbol{u}_1$ inside the solid. We define $\zeta = b/a$ as the non-dimensional radius of the pinned zone. Adopting the same spherical coordinate system, the solid pinned zone constraints of Eq. (1.43) read as

$$\begin{aligned} u_{1,r}|_{r=\zeta} &= 0 \\ u_{1,\theta}|_{r=\zeta} &= 0 \end{aligned} \tag{1.47}$$

while the solid–fluid interfacial stress boundary conditions of Eq. (1.46) become

$$\begin{aligned} \left.\frac{\partial v_{0,r}}{\partial r}\right|_{r=1} &= \frac{M^2}{\kappa}\left.\frac{\partial u_{1,r}}{\partial r}\right|_{r=1} \\ \left.\left(\frac{1}{r}\frac{\partial v_{0,r}}{\partial \theta} + \frac{\partial v_{0,\theta}}{\partial r} - \frac{v_{0,\theta}}{r}\right)\right|_{r=1} &= \frac{M^2}{\kappa}\left.\left(\frac{1}{r}\frac{\partial u_{1,r}}{\partial \theta} + \frac{\partial u_{1,\theta}}{\partial r} - \frac{u_{1,\theta}}{r}\right)\right|_{r=1}. \end{aligned} \tag{1.48}$$

We comment that Eq. (1.41) implies that $\boldsymbol{u}_1$ is divergence free, which allows the definition of a streamfunction-equivalent strain function $\boldsymbol{\varphi}_{e,1}$ where $\boldsymbol{u}_1 = \nabla \times \boldsymbol{\varphi}_{e,1}$. Taking the curl $(\nabla\times)$ of Eq. (1.42), and expressing $\boldsymbol{u}_1$ in terms of $\boldsymbol{\varphi}_{e,1}$, we obtain the following homogeneous fourth-order homogeneous biharmonic equation

$$\nabla^4 \boldsymbol{\varphi}_{e,1} = 0, \quad \boldsymbol{x} \in \Omega_e \tag{1.49}$$

with the pinned zone constraints Eq. (1.47) becoming

$$\begin{aligned} \left.\frac{1}{r\sin\theta}\frac{\partial(\varphi_{e,1}\sin\theta)}{\partial\theta}\right|_{r=\zeta} &= 0 \\ \left.-\frac{1}{r}\frac{\partial(r\varphi_{e,1})}{\partial r}\right|_{r=\zeta} &= 0. \end{aligned} \tag{1.50}$$

Next, the boundary conditions of Eq. (1.48), with forcing terms (i.e. previous order terms) moved to the RHS, become

$$\begin{aligned} &\left.\frac{\partial}{\partial r}\left(\frac{1}{r\sin\theta}\frac{\partial(\varphi_{e,1}\sin\theta)}{\partial\theta}\right)\right|_{r=1} = \frac{\kappa}{M^2}\left.\frac{\partial v_{0,r}}{\partial r}\right|_{r=1} \\ &\left.\left(\frac{1}{r}\frac{\partial}{\partial\theta}\left(\frac{1}{r\sin\theta}\frac{\partial(\varphi_{e,1}\sin\theta)}{\partial\theta}\right) - \frac{\partial}{\partial r}\left(\frac{1}{r}\frac{\partial(r\varphi_{e,1})}{\partial r}\right) + \frac{1}{r^2}\frac{\partial(r\varphi_{e,1})}{\partial r}\right)\right|_{r=1} \\ &= \frac{\kappa}{M^2}\left.\left(\frac{1}{r}\frac{\partial v_{0,r}}{\partial\theta} + \frac{\partial v_{0,\theta}}{\partial r} - \frac{v_{0,\theta}}{r}\right)\right|_{r=1}. \end{aligned} \tag{1.51}$$

The RHS of Eq. (1.51) can be directly evaluated using Eq. (1.36) and the recurrence properties of spherical Hankel functions, yielding

$$
\begin{aligned}
\left.\frac{\partial v_{0,r}}{\partial r}\right|_{r=1} &= -\frac{3\cos\theta}{2}\left(-3\frac{h_1(mr)}{m h_0(m) r^2} + \frac{h_0(mr)}{h_0(m)} + \frac{h_2(m)}{h_0(m) r^4}\right) e^{-it} + c.c.\Big|_{r=1} = 0 \\
\left.\frac{\partial v_{0,r}}{\partial \theta}\right|_{r=1} &= \frac{\sin\theta}{2}\left(3\frac{h_1(mr)}{m h_0(m) r} - 1 - \frac{h_2(m)}{r^3 h_0(m)}\right) e^{-it} + c.c.\Big|_{r=1} = 0 \\
\left.\frac{\partial v_{0,\theta}}{\partial r}\right|_{r=1} &= -\frac{3\sin\theta}{4}\left(-3\frac{h_1(mr)}{m h_0(m) r^2} + \frac{h_0(mr)}{h_0(m)} + \frac{m h_1(mr)}{h_0(m)} + \frac{h_2(m)}{h_0(m) r^4}\right) e^{-it} + c.c.\Big|_{r=1} \\
&= \sin\theta\, F(m)\, e^{-it} + c.c.
\end{aligned} \tag{1.52}
$$

Here, $F(m)$ expresses in compact form the terms in the parenthesis. Using Eq. (1.52), conditions of Eq. (1.51) simplify to

$$
\begin{aligned}
\left.\frac{\partial}{\partial r}\left(\frac{1}{r\sin\theta}\frac{\partial(\varphi_{e,1}\sin\theta)}{\partial\theta}\right)\right|_{r=1} &= 0 \\
\left.\left(\frac{1}{r}\frac{\partial}{\partial\theta}\left(\frac{1}{r\sin\theta}\frac{\partial(\varphi_{e,1}\sin\theta)}{\partial\theta}\right) - \frac{\partial}{\partial r}\left(\frac{1}{r}\frac{\partial(r\varphi_{e,1})}{\partial r}\right) + \frac{1}{r^2}\frac{\partial(r\varphi_{e,1})}{\partial r}\right)\right|_{r=1} &= \sin\theta\, F(m)\, e^{-it} + c.c.
\end{aligned} \tag{1.53}
$$

Now we have expressions for the four boundary conditions (pinned zone constraints - Eq. (1.50); solid–fluid interfacial stress boundary conditions - Eq. (1.53)) necessary to solve the elastic solid fourth order differential equation (Eq. 1.49). Based on the form of the boundary conditions in Eq. (1.53), we choose for the homogeneous biharmonic equation (Eq. (1.49)) the candidate general solution

$$
\varphi_{e,1} = \frac{\kappa}{M^2}\sin\theta\left(c_1 r + \frac{c_2}{r^2} + c_3 r^3 + c_4\right) F(m)\, e^{-it} + c.c. \tag{1.54}
$$

where c_1, c_2, c_3 and c_4 are constants that are determined from the 4 boundary conditions given by Eq. (1.50) and Eq. (1.53)

$$
\begin{aligned}
c_1\zeta + \frac{c_2}{\zeta^2} + c_3\zeta^3 + c_4 &= 0 \\
2c_1\zeta - \frac{c_2}{\zeta^2} + 4c_3\zeta^3 + c_4 &= 0 \\
-3c_2 + 2c_3 - c_4 &= 0 \\
-6(c_2 + c_3) &= 1.
\end{aligned} \tag{1.55}
$$

Solving the above linear system of equations yields

$$
\begin{aligned}
c_1 &= -\frac{9\zeta^4 + 9\zeta^3 + 4\zeta^2 + 4\zeta + 4}{6\zeta(\zeta - 1)\left(2\zeta^3 + 4\zeta^2 + 6\zeta + 3\right)} \\
c_2 &= -\frac{\zeta^2\left(\zeta^2 + \zeta + 1\right)}{3(\zeta - 1)\left(2\zeta^3 + 4\zeta^2 + 6\zeta + 3\right)} \\
c_3 &= \frac{\zeta + 1}{2(\zeta - 1)\left(2\zeta^3 + 4\zeta^2 + 6\zeta + 3\right)} \\
c_4 &= \frac{\zeta^4 + \zeta^3 + \zeta^2 + \zeta + 1}{(\zeta - 1)\left(2\zeta^3 + 4\zeta^2 + 6\zeta + 3\right)}.
\end{aligned} \tag{1.56}
$$

Having determined the strain function $\boldsymbol{\varphi}_{e,1}$, we proceed to evaluate $\boldsymbol{u}_1 = \boldsymbol{\nabla} \times \boldsymbol{\varphi}_{e,1}$ at the sphere surface ($r = 1$), which will eventually feed into the solution of the fluid phase through the no-slip boundary condition. The interfacial displacement $\boldsymbol{u}_1$, accurate up to $\mathcal{O}(\epsilon)$ is then given by

$$
\begin{aligned}
u_{1,r} = \frac{1}{r \sin\theta} \frac{\partial(\varphi_{e,1} \sin\theta)}{\partial\theta}\bigg|_{r=1} &= \frac{2\kappa}{M^2} \cos\theta \left(c_1 r + \frac{c_2}{r^2} + c_3 r^3 + c_4\right) F(m)\, e^{-it} + c.c.\bigg|_{r=1} \\
&= \frac{\kappa}{M^2} \cos\theta\, G_1(\zeta)\, F(m)\, e^{-it} + c.c. \\
u_{1,\theta} = -\frac{1}{r} \frac{\partial(r\varphi_{e,1})}{\partial r}\bigg|_{r=1} &= -\frac{\kappa}{M^2} \sin\theta \left(-2c_1 - \frac{c_2}{r^3} - 4c_3 r^2 - \frac{c_4}{r}\right) F(m)\, e^{-it} + c.c.\bigg|_{r=1} \\
&= -\frac{\kappa}{M^2} \sin\theta\, G_2(\zeta)\, F(m)\, e^{-it} + c.c.
\end{aligned}
\tag{1.57}
$$

with $G_1(\zeta)$ and $G_2(\zeta)$ as the compact notation for the bracketed terms.

We now have all the conditions required to evaluate the solution in the fluid phase at $\mathcal{O}(\epsilon)$. We recall that the governing equations in the fluid phase (Eq. (1.37)) can be written in vector potential form, which at $\mathcal{O}(\epsilon)$ read

$$
M^2 \frac{\partial \boldsymbol{\nabla}^2 \boldsymbol{\varphi}_1}{\partial t} + M^2 \left((\boldsymbol{v}_0 \cdot \boldsymbol{\nabla})\, \boldsymbol{\nabla}^2 \boldsymbol{\varphi}_0 \right) - M^2 \left((\boldsymbol{\nabla}^2 \boldsymbol{\varphi}_0 \cdot \boldsymbol{\nabla}) \boldsymbol{v}_0 \right) = \boldsymbol{\nabla}^4 \boldsymbol{\varphi}_1, \quad r \geqslant 1. \tag{1.58}
$$

where $\boldsymbol{v}_1 = \boldsymbol{\nabla} \times \boldsymbol{\varphi}_1$. We note that the term $M^2(\boldsymbol{\nabla}^2\boldsymbol{\varphi}_0 \cdot \boldsymbol{\nabla})\boldsymbol{v}_0$ in Eq. (1.58), which corresponds to vortex stretching, is absent in previous studies on rigid sphere streaming (Lane 1955). Thus, by considering this unaccounted term, our work significantly improves upon the rigid sphere streaming theory. In order to solve for φ_1, we first simplify the steady forcing forcing term $M^2 \left[(\boldsymbol{v}_0 \cdot \boldsymbol{\nabla})\, \boldsymbol{\nabla}^2 \varphi_0 - (\boldsymbol{\nabla}^2 \boldsymbol{\varphi}_0 \cdot \boldsymbol{\nabla}) \boldsymbol{v}_0 \right]$ with Eqs. (1.35) and (1.36)

$$
M^2 \left[(\boldsymbol{v}_0 \cdot \boldsymbol{\nabla})\, \boldsymbol{\nabla}^2 \varphi_0 - (\boldsymbol{\nabla}^2 \boldsymbol{\varphi}_0 \cdot \boldsymbol{\nabla}) \boldsymbol{v}_0 \right] = \sin 2\theta \left(\rho(r) + \Omega(r) e^{-it} + \Omega^*(r) e^{it} \right) \tag{1.59}
$$

where

$$
\begin{aligned}
\rho(r) &= \frac{1}{16 r^4} \left(r^3 J^{(3)} + r^2 J^{(2)} - 6 r J^{(1)} + 6J \right) J^* + c.c. \\
J(r) &= 3 \frac{h_1(mr)}{m h_0(m)} - r - \frac{h_2(m)}{r^2 h_0(m)}
\end{aligned}
\tag{1.60}
$$

Here J is the radially dependent term in Eq. (1.35), with $J^{(n)}$ and J^* being its n^{th} derivative and complex conjugate, respectively. The terms $\sin 2\theta\, \Omega(r) e^{2it}$ and $\sin 2\theta\, \Omega(r) e^{-2it}$ correspond to higher order oscillatory forcing terms, which generate oscillatory unsteady corrections to the first order flow. In contrast, the term $\sin 2\theta \rho(r)$ is real, steady, time-independent and is the one responsible for the streaming flow that emerges in the case of a rigid sphere, as demonstrated previously in Lane (1955). Since we are interested in steady streaming flow, we consider the time-averaged form of Eq. (1.58) (i.e. dropping the time derivative), yielding

$$
\boldsymbol{\nabla}^4 \langle \boldsymbol{\varphi}_1 \rangle = \sin 2\theta\, \rho(r)\, \hat{\boldsymbol{\phi}}, \quad r \geqslant 1 \tag{1.61}
$$

where $\langle \cdot \rangle$ stands for a time averaged field. To solve the above equation in the fluid phase, we recall the necessary no-slip boundary conditions given in Eq. (1.23) that needs to be enforced at the elastic solid–fluid interface, deformed by the zeroth order flow. Based on Eq. (1.57), we note that $r = 1 + \epsilon u_{1,r}$ corresponds to an $\mathcal{O}(\epsilon)$ accurate expression for the location of the deforming interface. The no-slip condition of Eq. (1.23) can then be written as

$$\begin{aligned} v_{f,r}\big|_{\partial\Omega} &= v_{f,r}\big|_{r=1+\epsilon u_{1,r}} + \mathcal{O}\left(\epsilon^2\right) &&= v_{e,r}\big|_{\partial\Omega} &&= v_{e,r}\big|_{r=1+\epsilon u_{1,r}} + \mathcal{O}\left(\epsilon^2\right) \\ v_{f,\theta}\big|_{\partial\Omega} &= v_{f,\theta}\big|_{r=1+\epsilon u_{1,r}} + \mathcal{O}\left(\epsilon^2\right) &&= v_{e,\theta}\big|_{\partial\Omega} &&= v_{e,\theta}\big|_{r=1+\epsilon u_{1,r}} + \mathcal{O}\left(\epsilon^2\right) \end{aligned} \tag{1.62}$$

where the subscripts e and f refer to the interfacial field values from the elastic solid and fluid perspective, respectively. The RHS of Eq. (1.62) is the deformation velocity of the elastic solid interface, which can be computed from the displacement field $\boldsymbol{u}$ of Eq. (1.57) as

$$\begin{aligned} v_{e,r}\big|_{\partial\Omega} &= \left.\frac{\partial u_r}{\partial t}\right|_{r=1+\epsilon u_{1,r}} + \mathcal{O}\left(\epsilon^2\right) = \left.\frac{\partial(\epsilon u_{1,r} + \mathcal{O}\left(\epsilon^2\right))}{\partial t}\right|_{r=1+\epsilon u_{1,r}} + \mathcal{O}\left(\epsilon^2\right) \\ &= \left.\frac{\partial(\epsilon u_{1,r} + \mathcal{O}\left(\epsilon^2\right))}{\partial t}\right|_{r=1} + \epsilon u_{1,r} \left.\frac{\partial^2(\epsilon u_{1,r} + \mathcal{O}\left(\epsilon^2\right))}{\partial r \partial t}\right|_{r=1} + \mathcal{O}\left(\epsilon^2\right) \\ &= \epsilon \left.\frac{\partial u_{1,r}}{\partial t}\right|_{r=1} + \mathcal{O}\left(\epsilon^2\right) \\ &= -\epsilon i \frac{\kappa}{M^2} \cos\theta \; G_1(\zeta) \; F(m) \; e^{-it} + c.c. + \mathcal{O}\left(\epsilon^2\right) \\ v_{e,\theta}\big|_{\partial\Omega} &= \left.\frac{\partial u_\theta}{\partial t}\right|_{r=1+\epsilon u_{1,r}} + \mathcal{O}\left(\epsilon^2\right) = \left.\frac{\partial(\epsilon u_{1,\theta} + \mathcal{O}\left(\epsilon^2\right))}{\partial t}\right|_{r=1+\epsilon u_{1,r}} + \mathcal{O}\left(\epsilon^2\right) \\ &= \left.\frac{\partial(\epsilon u_{1,\theta} + \mathcal{O}\left(\epsilon^2\right))}{\partial t}\right|_{r=1} + \epsilon u_{1,r} \left.\frac{\partial^2(\epsilon u_{1,\theta} + \mathcal{O}\left(\epsilon^2\right))}{\partial r \partial t}\right|_{r=1} + \mathcal{O}\left(\epsilon^2\right) \\ &= \epsilon \left.\frac{\partial u_{1,\theta}}{\partial t}\right|_{r=1} + \mathcal{O}\left(\epsilon^2\right) \\ &= -\epsilon i \frac{\kappa}{M^2} \sin\theta \; G_2(\zeta) \; F(m) \; e^{-it} + c.c. + \mathcal{O}\left(\epsilon^2\right). \end{aligned} \tag{1.63}$$

We note that at zeroth order the displacement field is zero ($u_{0,r} = u_{0,\theta} = 0$), hence $u_r = \epsilon u_{1,r} + \mathcal{O}\left(\epsilon^2\right)$ and $u_\theta = \epsilon u_{1,\theta} + \mathcal{O}\left(\epsilon^2\right)$. There are now two ways to enforce the no-slip condition of Eq. (1.44) to the fluid. First, we can adopt a moving coordinate system attached to the moving interface, and enforce the no-slip condition on a fixed surface in that frame of reference. Second, we can maintain the fixed coordinate system with origin at the sphere center, and enforce the no-slip condition on a moving interface. Since the use of moving coordinates presents technical complications in the time averaging process eventually needed for streaming, as pointed out in Longuet-Higgins (1998), we adopt the latter approach. Additionally, we can replace the boundary flow velocity $v_{f,r}|_{r=1+\epsilon u_{1,r}}$ and $v_{f,\theta}|_{r=1+\epsilon u_{1,r}}$ on the temporally moving interface $r = 1+\epsilon u_{1,r}$ with the velocity that the flow would need to see on the fixed interface $r = 1$ to respond equivalently. This boundary condition transfer can be achieved by Taylor expanding $v_{f,r}|_{r=1+\epsilon u_{1,r}}$ and $v_{f,\theta}|_{r=1+\epsilon u_{1,r}}$ about $r = 1$ (Longuet-Higgins

1998)

$$
\begin{aligned}
v_{f,r}|_{\partial\Omega} = v_{f,r}|_{r=1+\epsilon u_{1,r}} + O\left(\epsilon^2\right) &= \left(v_{f,r} + \frac{\partial v_{f,r}}{\partial r}\left(\epsilon u_{1,r} + O\left(\epsilon^2\right)\right)\right)\Big|_{r=1} + O\left(\epsilon^2\right) \\
&= \left(v_{f,r} + \epsilon\frac{\partial v_{f,r}}{\partial r}u_{1,r}\right)\Big|_{r=1} + O\left(\epsilon^2\right) \\
v_{f,\theta}|_{\partial\Omega} = v_{f,\theta}|_{r=1+\epsilon u_{1,r}} + O\left(\epsilon^2\right) &= \left(v_{f,\theta} + \frac{\partial v_{f,\theta}}{\partial r}\left(\epsilon u_{1,r} + O\left(\epsilon^2\right)\right)\right)\Big|_{r=1} + O\left(\epsilon^2\right) \\
&= \left(v_{f,\theta} + \epsilon\frac{\partial v_{f,\theta}}{\partial r}u_{1,r}\right)\Big|_{r=1} + O\left(\epsilon^2\right).
\end{aligned}
\tag{1.64}
$$

To avoid subscript clutte, we henceforth drop the subscript f, and all references of the velocity field $\boldsymbol{v}$ now correspond to the velocity in the fluid phase. By combining Eqs. (1.62) to (1.64), followed by substitution of the asymptotic series for fluid velocity $\boldsymbol{v} = \boldsymbol{v}_0 + \epsilon\boldsymbol{v}_1 + O\left(\epsilon^2\right)$ and retention of $O\left(\epsilon\right)$ terms, we obtain

$$
\begin{aligned}
\left(v_{1,r} + \frac{\partial v_{0,r}}{\partial r}u_{1,r}\right)\Big|_{r=1} &= -i\frac{\kappa}{M^2}\cos\theta\, G_1(\zeta)\, F(m)\, e^{-it} + c.c. \\
\left(v_{1,\theta} + \frac{\partial v_{0,\theta}}{\partial r}u_{1,r}\right)\Big|_{r=1} &= -i\frac{\kappa}{M^2}\sin\theta\, G_2(\zeta)\, F(m)\, e^{-it} + c.c.
\end{aligned}
\tag{1.65}
$$

The first term on LHS of the equation above ($\boldsymbol{v}_1|_{r=1}$), currently unknown, corresponds to the first-order no-slip velocity that the fluid flow experiences at the zeroth-order boundary $r = 1$ due to the boundary condition transfer. The second term on the LHS, which represents the correction generated due to the Taylor expansion, can be evaluated using Eq. (1.52) and Eq. (1.57) as

$$
\begin{aligned}
\left(\frac{\partial v_{0,r}}{\partial r}u_{1,r}\right)\Big|_{r=1} &= 0 \\
\left(\frac{\partial v_{0,\theta}}{\partial r}u_{1,r}\right)\Big|_{r=1} &= \frac{\kappa}{M^2}\sin 2\theta\,\left(G_1(\zeta)F(m)F^*(m) + \phi(r)e^{-2it} + \phi^*(r)e^{2it}\right).
\end{aligned}
\tag{1.66}
$$

Since we are interested in the effect of elasticity on steady streaming flow, we consider the time averaged form of the no-slip condition of Eq. (1.65), which via Eq. (1.66) reduces to

$$
\begin{aligned}
\langle v_{1,r}\rangle\big|_{r=1} &= 0 \\
\langle v_{1,\theta}\rangle\big|_{r=1} &= -\frac{\kappa}{M^2}\sin 2\theta\, G_1(\zeta)F(m)F^*(m).
\end{aligned}
\tag{1.67}
$$

Equation (1.67) suggests that an oscillatory no-slip velocity imposed on a moving interface ($r = 1 + \epsilon u_{1,r}$) can be equivalently seen as a rectified slip different from zero ($\langle v_{1,\theta}\rangle|_{r=1} \neq 0$) at the zeroth-order, fixed interface $r = 1$. Such rectified slip velocities are also seen in the case of streaming flow generation due to axisymmetric pulsating bubbles (Longuet-Higgins 1998; Spelman & Lauga 2017). In our case this slip velocity, which is non-zero only for a deformable elastic body, modifies the well-known steady streaming flow generated due to the Reynolds stress term ($\sin 2\theta\ \rho(r)$, RHS of Eq. (1.61)) induced by the rigid sphere counterpart. We remark that this slip is independent of the nonlinear inertial advection term in Navier–Stokes equations, and thus can generate streaming even in the Stokes limit, unlike the case of rigid bodies. Finally, to derive the effect of this steady slip on streaming flow, we consider the vector potential form of the time averaged no-slip condition Eq. (1.67)

$$\begin{aligned} \frac{1}{r\sin\theta}\frac{\partial(\langle\varphi_1\rangle\sin\theta)}{\partial\theta}\bigg|_{r=1} &= 0 \\ \frac{1}{r}\frac{\partial(r\langle\varphi_1\rangle)}{\partial r}\bigg|_{r=1} &= \frac{\kappa}{M^2}\sin 2\theta\, G_1(\zeta)F(m)F^*(m) \end{aligned} \tag{1.68}$$

where $\boldsymbol{\varphi}_1 = \boldsymbol{\nabla}\times\boldsymbol{v}_1$. Similarly, the time averaged far-field conditions from Eq. (1.26), read

$$\begin{aligned} \frac{1}{r\sin\theta}\frac{\partial(\langle\varphi_1\rangle\sin\theta)}{\partial\theta}\bigg|_{r\to\infty} &= 0 \\ \frac{1}{r}\frac{\partial(r\langle\varphi_1\rangle)}{\partial r}\bigg|_{r=\to\infty} &= 0. \end{aligned} \tag{1.69}$$

Finally, with the time averaged flow of equation Eq. (1.61) and the necessary boundary conditions of Eq. (1.68) and Eq. (1.69) resolved, the steady streaming flow solution for a weakly elastic sphere can be computed to $\mathcal{O}(\epsilon)$ accuracy, yielding

$$\langle\varphi_1\rangle = \sin 2\theta\ \left[\Theta(r) + \Lambda(r)\right] \tag{1.70}$$

where $\Theta(r)$ is the rectified classical rigid body contribution

$$\begin{aligned} \Theta(r) = &-\frac{r^4}{70}\int_r^\infty \frac{\rho(\tau)}{\tau}\,\mathrm{d}\tau + \frac{r^2}{30}\int_r^\infty \tau\rho(\tau)\,\mathrm{d}\tau \\ &+ \frac{1}{r}\left(\frac{1}{30}\int_1^r \tau^4\rho(\tau)\,\mathrm{d}\tau + \frac{1}{20}\int_1^\infty \frac{\rho(\tau)}{\tau}\,\mathrm{d}\tau - \frac{1}{12}\int_1^\infty \tau\rho(\tau)\,\mathrm{d}\tau\right) \\ &+ \frac{1}{r^3}\left(-\frac{1}{70}\int_1^r \tau^6\rho(\tau)\,\mathrm{d}\tau - \frac{1}{28}\int_1^\infty \frac{\rho(\tau)}{\tau}\,\mathrm{d}\tau + \frac{1}{20}\int_1^\infty \tau\rho(\tau)\,\mathrm{d}\tau\right) \end{aligned} \tag{1.71}$$

whose asymptotic nature is given by

$$\begin{aligned} \Theta(\infty) &= 0 \\ \frac{d\Theta}{dr}(\infty) &= 0 \end{aligned} \tag{1.72}$$

Next, $\Lambda(r)$ is the new elasticity effect modification given by

$$\Lambda(r) = 0.5\frac{\kappa}{M^2}\,G_1(\zeta)F(m)F^*(m)\left(\frac{1}{r} - \frac{1}{r^3}\right) \tag{1.73}$$

whose asymptotic nature is given by

$$\begin{aligned} \Lambda(\infty) &= 0 \\ \frac{d\Lambda}{dr}(\infty) &= 0 \end{aligned} \tag{1.74}$$

$G_1(\zeta)$ and $F(m)$ are expanded here for convenience

$$\begin{aligned} G_1(\zeta) &= \frac{(\zeta-1)^2\left(4\zeta^2+7\zeta+4\right)}{3\zeta\left(2\zeta^3+4\zeta^2+6\zeta+3\right)} \\ F(m) &= -\frac{3mh_1(m)}{4h_0(m)} \end{aligned} \tag{1.75}$$

This concludes the detailed, step-by-step derivation of the viscous streaming solution for the case of a hyperelastic three-dimensional sphere.

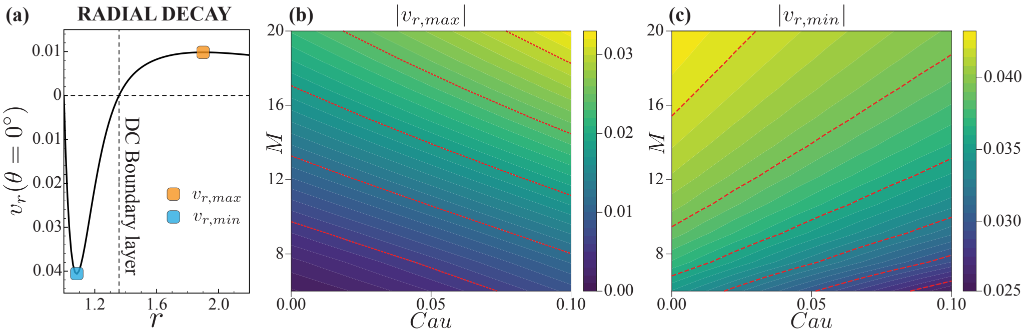

Figure 2: Effect of elasticity on streaming flow strength. (a) Radial variation of radial Eulerian velocity v_r along $\theta = 0°$ for $M = 12$ and Cau = 0 (rigid limit). Orange and blue markers correspond to the maximum ($v_{r,max}$) and minimum ($v_{r,min}$) velocities, respectively. (b, c) Heat-maps tracking $|v_{r,max}|$ and $|v_{r,min}|$ as functions of M and Cau. Red dashed lines are iso-contours.

2. Stokes drift correction

The final result of Eq. 3.20 in the main text represents the Eulerian vector potential for the steady streaming flow. However, fluid particles do not precisely follow the corresponding streamlines because of Stokes drift. This implies that true pathlines of fluid particles, i.e. the Lagrangian streamlines, require the computation of the Stokes drift to correct the Eulerian counterparts. Following the derivation in supplementary material §3 of Bhosale *et al.* (2022), we derive the Lagrangian vector potential as

$$\langle \varphi_1^L \rangle = \langle \varphi_1 \rangle + \sin 2\theta \, \beta(r) \tag{2.1}$$

where φ_1 is the azimuthal component of Eulerian vector potential in main text (Eq. 3.20) and

$$\beta(r) = \frac{3}{8}\mathrm{Im}\left[\frac{h_0(mr)h_2(mr)^*}{h_0(m)h_0(m)^*} + \frac{h_2(mr)}{h_0(m)} + \frac{h_2(m)h_0(mr)^*}{r^3 h_0(m)h_0(m)^*} - \frac{h_2(m)}{r^3 h_0(m)}\right] \tag{2.2}$$

Here, $m = \sqrt{i}M$, with h_n, *, M and $\mathrm{Im}[\cdot]$ referring to the n^{th} order Hankel function of the first kind, complex conjugate, Womersley number and the imaginary part, respectively.

3. Effect of elasticity on flow strength

In this section, we present how variations in flow inertia (M) and sphere elasticity (Cau) affect the flow strength of the resulting streaming field. Following classical streaming literature (Bertelsen *et al.* (1973)), we characterize the flow strength via the Eulerian velocity along $\theta = 0°$. Since the tangential component of the velocity is $v_\theta = 0$ along $\theta = 0°$, we can equivalently characterize the flow strength via the radial velocity v_r. Figure 2a shows a typical variation of $v_r(\theta = 0°)$ for Cau = 0 (rigid limit) and $M = 12$. To characterize flow strength consistently, in Fig. 2b, c we track maximum ($v_{r,max}$, orange marker, Fig. 2b) and minimum ($v_{\theta,min}$, blue marker, Fig. 2c) velocities as functions of Cau and M. As seen in Fig. 2(b), $|v_{r,max}|$ increases with both sphere elasticity (Cau) and flow inertia (M). In Fig. 2(c), instead, $|v_{r,min}|$ increases with M but decreases with Cau. The above analysis provides a compact rulebook to manipulate streaming flow strength, via variations in flow inertia (M) and sphere elasticity (Cau).

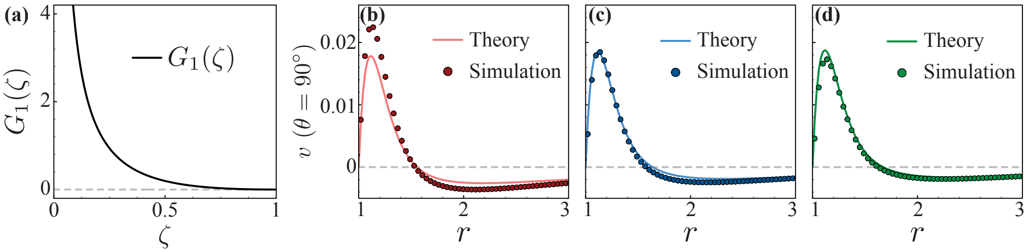

Figure 3: Effect of pinned zone radius ζ on streaming flow. (a) Prefactor $G_1(\zeta)$, which captures the ζ-dependence of the elastic streaming modification term $\Lambda(r)$, versus pinned zone radius ζ. (b-d) Radial decay of velocity magnitude along $\theta = 90^\circ$ at $M = 8$, for elastic spheres with Cau = 0.025 and varying pinned zone radius (b) $\zeta = 0.4$, (c) $\zeta = 0.6$, and (d) $\zeta = 0.8$.

4. Effect of pinned zone radius on streaming flow

In this section, we demonstrate the effects of pinned zone radius ζ of the soft sphere on the resultant streaming flow. We first consider the elasticity-based streaming modification term $\Lambda(r)$, and specifically the prefactor $G_1(\zeta)$, which captures the ζ-dependence of $\Lambda(r)$. Figure 3(a) shows the variation of $G_1(\zeta)$ with ζ, where $G_1(\zeta)$ is observed to decrease with increasing ζ. The term $G_1(\zeta)$ asymptotically approaches zero as $\zeta \rightarrow 1$, which implies that the entire sphere is treated as pinned zone rendering the sphere rigid, and thus body elasticity does not affect the streaming flow. On the other hand, as $\zeta \rightarrow 0$, a singularity is observed for $G_1(\zeta) \rightarrow \infty$. This represents a physically unrealistic scenario where the soft sphere is 'pinned' in a region of zero thickness. For a realistic range of pinned zone radii ζ, theory predicts that decreasing the pinned zone radius ζ leads to an increase in the elastic contribution to streaming (Fig. 3a), as intuitively expected.

We next proceed to validate the above theoretical predictions by comparing against results from numerical simulations. With body softness (Cau = 0.025) and flow inertia ($M = 8$) fixed, we increase the pinned zone radius ζ and observe its effect on streaming, characterized via the radial velocity decay along $\theta = 90^\circ$ (Fig. 3(b-d)). We note the close agreement between theoretical predictions and the numerical results. Figure 3(b-d) further shows that, with increasing pinned zone radius ζ, there is an increase in δ_{DC}, which approaches the flow configuration of a rigid sphere as $\zeta \rightarrow 1$. This shows that the pinned zone radius can be utilized as an additional, tunable parameter to rationally modulate streaming flow topology via elasticity.

5. Equivalent experimental parameters

Here, we report the range of realistic experimental parameters, equivalent to the values of M, ϵ and Cau considered in the main text, for which body elasticity significantly affects streaming. The non-dimensional quantities (M, ϵ and Cau) and corresponding experimental parameter ranges are tabulated in Table 1. For streaming setup properties that include fluid density ρ_f, angular oscillation frequency ω, fluid kinematic viscosity ν and sphere radius a, we assume ranges typically employed in streaming applications (Lutz *et al.* 2005, 2006; Vishwanathan & Juarez 2019; Bhosale *et al.* 2021*b*). Then, we derive ranges for the shear modulus G of the body, showcased in the last row of Table 1. As seen from Table 1, the shear modulus (G) range corresponds to materials that can be realistically employed in microfluidic settings, from soft biological tissues (Liu *et al.* 2015) to common polymeric materials such as Polydimethylsiloxane (PDMS) (Lötters *et al.* 1997; Wang *et al.* 2014). We

Parameter	Value range
	Non-dimensional quantities
M	$\mathcal{O}(1) - \mathcal{O}(10)$
ϵ	$\mathcal{O}\left(10^{-1}\right)$
Cau	$\mathcal{O}\left(10^{-1}\right)$
	Equivalent experimental quantities
ρ_f	$\mathcal{O}\left(10^{3}\right)$ $\mathrm{kg \cdot m^{-3}}$ (Lutz *et al.* 2005; Vishwanathan & Juarez 2019; Bhosale *et al.* 2021*b*)
ν	$\mathcal{O}\left(10^{-6}\right)$ $\mathrm{m^2 \cdot s^{-1}}$ (Lutz *et al.* 2005; Vishwanathan & Juarez 2019; Bhosale *et al.* 2021*b*)
a	$\mathcal{O}\left(10^{-4}\right) - \mathcal{O}\left(10^{-3}\right)$ m (Lutz *et al.* 2005; Vishwanathan & Juarez 2019; Bhosale *et al.* 2021*b*)
ω	$\mathcal{O}\left(10^{2}\right) - \mathcal{O}\left(10^{3}\right)$ $\mathrm{rad \cdot s^{-1}}$ (Lutz *et al.* 2005; Vishwanathan & Juarez 2019; Bhosale *et al.* 2021*b*)
G	$\mathcal{O}(1) - \mathcal{O}\left(10^{2}\right)$ kPa

Table 1: Range of realistic experimental parameters for which body elasticity significantly affects streaming.

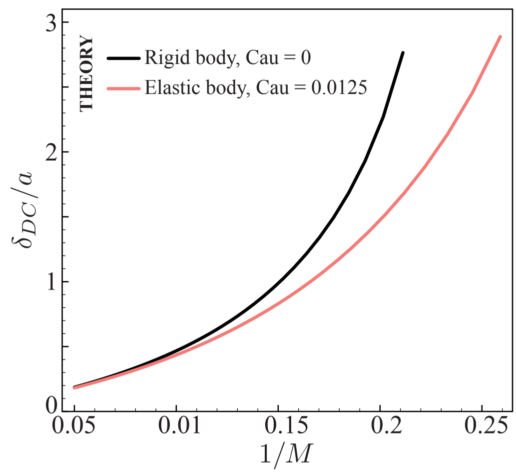

Figure 4: Normalized DC layer thickness δ_{DC}/a vs. inverse of Womersley number ($1/M$) from theory, for rigid (Cau = 0) and elastic (Cau = 0.0125) spheres.

conclude that within the range of experimental parameters shown in Table 1, body elasticity can be realistically used to significantly modulate streaming flows.

6. Behavior of δ_{DC} with M in the limit $M \to \mathcal{O}(1)$

To investigate the behavior of δ_{DC} with M for a soft sphere, in the low inertia limit i.e. for $M \to \mathcal{O}(1)$, we extend the range of M considered in the main text (Fig. 2d), and present the corresponding theoretically predicted DC layer thickness δ_{DC}/a values in Fig. 4. As it can be seen, approach to divergence is observed for Cau > 0, although at values of M lower than those of the rigid sphere limit. This is expected since, for Cau > 0, the rigid body

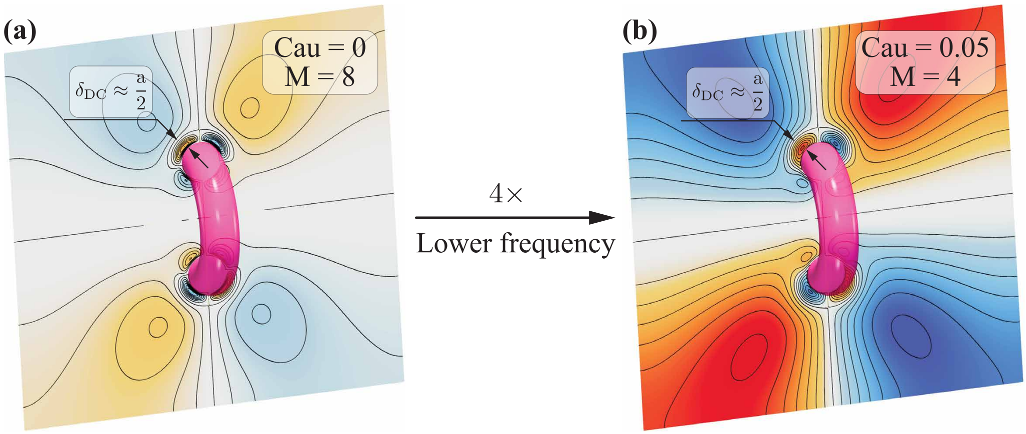

Figure 5: Frequency reduction to achieve the same flow topology via elasticity for a 3D torus. Stokes streamfunctions contours are shown for (a) a rigid torus with Cau = 0, M = 8 and (b) a elastic torus with Cau = 0, M = 8 (see main text Fig. 3 captions for details). DC layer thicknesses, similarly defined as the soft sphere case, is included for reference.

contribution $\Theta(r)$ is the same as in classic streaming and will diverge, with the elasticity contribution $\Lambda(r)$ only shifting the curve.

7. Frequency reduction via elasticity in multi-curvature bodies

Here we demonstrate that similar flow topologies for an elastic torus with Cau = 0.05, $M = 4$ (Fig. 5b, main text Fig.3c), characterized by close agreement in DC layer thicknesses (δ_{DC}), can be alternatively obtained by using its rigid counterparts (Fig. 5a). However, this requires 4 times higher oscillation frequency ω, as suggested by the doubling in Womersley number M. This underlines the distinct advantage in leveraging body compliance for viscous streaming, where the same flow topology can be achieved at a significantly lower frequency via the use of body elasticity.

8. *Details regarding the sphere streaming simulation*

*We elaborate in this section a number of implementation details concerning the sphere streaming simulation (main text Fig. 2, supplementary materials Fig. 6). First, we briefly justify the usage of pinned zone radius $\zeta = 0.4$. Lowering the pinned zone radius rapidly increases the prefactor $G_1(\zeta)$ (main text Eq. 3.19, supplementary materials Eq. 1.75), which results in a slip velocity much greater than $O(1)$, thereby weakening the asymptotic assumption. The opposite holds true for large ζ, rendering $\zeta = 0.4$ a robust compromise. Next, we characterize streaming via the thickness of the DC layer, which refers to the innermost recirculation zone, for its utility in trapping, filtration and chemical mixing, and because of its robust nature. Regarding the numerical implementation, the simulations are performed using a vortex-method based formulation (*Gazzola et al. 2011; Bhosale et al. 2021a, 2023*) that solves the vorticity form of the Navier–Stokes equations in an axisymmetric cylindrical coordinate system. Within this framework, fluid and solid are modeled to be density matched ($\rho_f = \rho_e = 1$). The rigid sphere and pinned zone are modeled as Brinkman solids, and the elastic phase as a viscoelastic Kelvin-Voigt solid with shear modulus G. Soft body deformations are tracked using an inverse-map technique (*Bhosale et al. 2021a; Kamrin & Nave 2009; Kamrin et al. 2012*). The far-field velocity is $V(t) = V_0 \cos \omega t$ with characteristic*

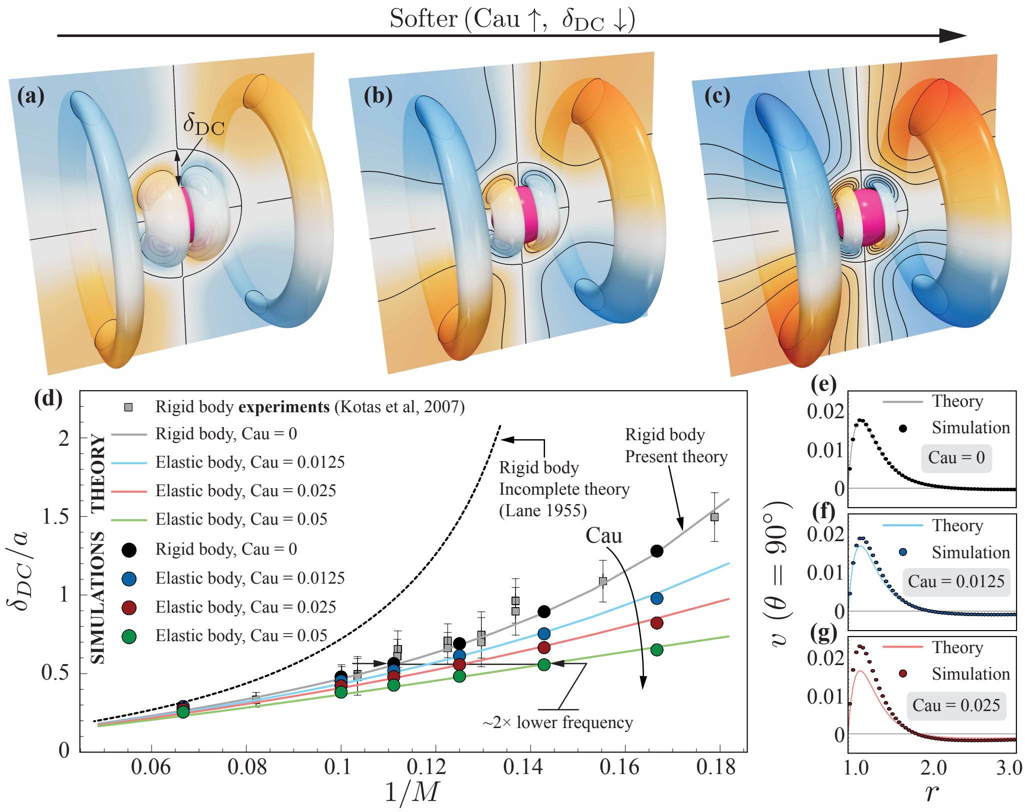

Figure 6: **Elastic sphere and streaming flow response. (a-c)** 3D time-averaged Lagrangian (i.e. Stokes-drift corrected, supplementary material §3) Stokes streamfunction depicting the streaming response at $M = 6$ with increasing softness Cau. (a) Rigid limit Cau = 0, (b) Cau = 0.025, and (c) Cau = 0.05. Note that blue/orange represent clockwise/counterclockwise rotating regions. The non-dimensional radius of the pinned zone is set at $\zeta = 0.4$ throughout the study, to maintain the tangential slip velocity magnitude (Eq. **??**) at $O(1)$, consistent with the asymptotic analysis. The effect of pinned zone radius on streaming flow is detailed in Section §4 of the supplementary material. **(d)** Normalized DC layer thickness (δ_{DC}/a) vs. inverse Womersley number ($1/M$) from theory and simulations, for varying body elasticity Cau. An alternative theory (purple dashed line) derived by Riley (1966), the incomplete theory (black dashed line) of Lane (1955), and experimental results (grey squares) (Kotas *et al.* 2007) in the rigidity limit are plotted for reference. **(e-g)** Radial decay of velocity magnitude along $\theta = 90°$ from theory and simulations at $M = 6$, with increasing softness Cau. (e) Rigid limit Cau = 0, (f) Cau = 0.0125, and (g) Cau = 0.025.

velocity $V_0 = \epsilon a \omega$*, where* $\epsilon = 0.1$*,* $a = 0.1$*, and* $\omega = 32\pi$*. The fluid dynamic viscosity* μ_f *and elastic body's shear modulus* G *are determined based on the Womersley number* $M = a\sqrt{\rho_f \omega/\mu_f}$ *and Cauchy number* $\mathrm{Cau} = \epsilon \rho_f a^2 \omega^2 / G$*. Additional simulation parameters include: domain* $[0, 1] \times [0, 0.5]$*, uniform grid spacing* $h = 1/1024$*, Brinkman penalization factor* $\lambda = 1e6$*, mollification length* $\epsilon_{moll} = 2h$*, Courant–Friedrichs–Lewy number CFL* $= 0.1$*. For details on these parameters, refer to (Gazzola* et al. *2011; Bhosale* et al. *2021a; Parthasarathy* et al. *2022; Bhosale* et al. *2023).*

9. *Rigid sphere streaming solution by* Riley *(1966)*

*In this section, we elaborate upon the rigid sphere streaming solution derived by (*Riley *1966), where an inner-outer asymptotic expansion approach is employed.*

First, we note a number of key differences in assumptions and nomenclature between Riley's work and the present theory. Riley formulates the Navier-Stokes equation in the Stokes-streamfunction (ψ) form, where the radial and tangential velocities are evaluated as

$$v_r = \frac{1}{r^2 \sin\theta}\frac{\partial\psi}{\partial\theta}, \quad v_\theta = -\frac{1}{r\sin\theta}\frac{\partial\psi}{\partial r} \tag{9.1}$$

whereas the vector potential $\boldsymbol{\varphi}$ is used in the present work, with velocities given in Eq. (1.36). We note that in spherical coordinates, the azimuthal vector potential may be directly recovered from corresponding Stokes streamfunction by

$$\varphi = \boldsymbol{\varphi}\cdot\hat{\boldsymbol{\phi}} = \frac{\psi}{r\sin\theta} \tag{9.2}$$

Furthermore, Riley considers the nondimensional far-field boundary condition

$$\psi|_{r\to\infty} = \frac{1}{2}r^2\sin^2\theta e^{it} \tag{9.3}$$

which in velocity form (using Eq. (9.1)) reduces to

$$\boldsymbol{v}|_{r\to\infty} = e^{it}\hat{\boldsymbol{\imath}} \tag{9.4}$$

where $\hat{\boldsymbol{\imath}}$ is the oscillation direction similarly defined in Eq. (1.8). The pure-cosine farfield boundary condition used in this work (Eq. (1.16)) is recovered by taking the real part of Eq. (9.4). Finally, Riley characterizes the inertia-viscous regimes via an imaginary nondimensional number that is closely related to the Womersley number

$$m^2 = i\frac{\omega a^2}{\nu} \quad \Leftrightarrow \quad m = \frac{1+i}{\sqrt{2}}M \tag{9.5}$$

where m is also used in depicting the zeroth-order unsteady streaming solution in the present theory (Eq. (1.35)). For consistency in nomenclature, we exclusively use the Womersley number M in the following formulation of Riley's theory.

Riley's theory considers two different regimes, one where the Womersley number is small $M^2 \ll 1$ (viscous regime) and one where $M^2 \gg 1$ (inertial regime). Our theory instead assumes $M \sim \mathcal{O}(1)$, corresponding to an intermediate inertial-viscous regime, one which is of practical experimental relevance (Section 5). Within this context, we discuss how Riley's limits fare when applied to the $M \sim \mathcal{O}(1-10)$ regime, which is the focus of this study. At $M^2 \ll 1$ (viscous regime), both Riley and the present theory (Section 6) predicts an unbounded δ_{DC} (corresponding to the far top-right region of Fig. 7) and therefore cannot be compared to our theory in the viscous-inertial regime where a finite δ_{DC} is present. Riley's theory for $M^2 \gg 1$ instead predicts the presence of a bounded DC layer, allowing us to quantitatively compare with our results. In Riley's theory, a uniformly valid solution for the entire flow domain is not provided; instead, individual inner and outer solutions with appropriate matching conditions are formulated. The inner-solution to the first-order ($\mathcal{O}(\epsilon)$) time-averaged streamfunction reads

$$\langle\psi_1^{(in)}\rangle = \frac{9\sqrt{2}}{4M}\left(\frac{1}{8}e^{-2\eta} + \frac{5}{2}e^{-2\eta}\cos\eta + \frac{3}{2}e^{-\eta}\sin\eta + \eta e^{-\eta}\sin\eta - \frac{21}{8} + \frac{5}{4}\eta\right)\cos\theta\sin^2\theta \tag{9.6}$$

where

$$\eta = \frac{M(r-1)}{\sqrt{2}}$$

The steady outer-layer equation, under the assumption of $\epsilon^2 M^2 \ll 1$, is governed by a homogeneous biharmonic equation with solution of the form

$$\langle \psi_1^{(out)} \rangle = \left(\frac{A_1}{r^2} + B_1 \right) \cos\theta \sin^2\theta \tag{9.7}$$

Riley unifies the inner (Eq. (9.6)) and outer (Eq. (9.7)) layer solutions by equating them in the limit of $r \to \infty$, where the solutions become

$$\begin{aligned} \langle \psi_1^{(in)} \rangle|_{r\to\infty} &= \frac{9\sqrt{2}}{4M} \left(-\frac{21}{8} + \frac{5}{4}\eta \right) \cos\theta \sin^2\theta \\ \langle \psi_1^{(out)} \rangle|_{r\to\infty} &= \left(A_1 + B_1 - \frac{2\sqrt{2}}{M} A_1 \eta \right) \cos\theta \sin^2\theta \end{aligned} \tag{9.8}$$

where they obtain the coefficients by matching the the two limits

$$A_1 = -\frac{45}{32}, \quad B_1 = \frac{45}{32} \tag{9.9}$$

Here we remark that the first terms of the two equations cannot be matched due to the differences in orders of magnitude ($O(1)$ vs. $O(1/M)$).

While Riley provided the appropriate matching conditions, a uniformly valid solution for the entire fluid domain is not explicitly stated. Hence, following Riley's solution we derive here the complementary solution that combines the inner and outer expansions. A direct result from the matching (Eq. (9.8)) is the shared limit terms between the inner and outer solutions

$$\langle \psi_1^{(s)} \rangle = \frac{45\sqrt{2}}{16M} \eta \tag{9.10}$$

The unified, first-order steady streaming solution from Riley's formulation is obtained by combining the inner and outer solutions while subtracting the shared terms

$$\begin{aligned} \langle \psi_1 \rangle &= \langle \psi_1^{(in)} \rangle + \langle \psi_1^{(out)} \rangle - \langle \psi_1^{(s)} \rangle \\ &= \left[\frac{9\sqrt{2}}{4M} \left(\frac{1}{8} e^{-2\eta} + \frac{5}{2} e^{-\eta} \cos\eta + \frac{3}{2} e^{-\eta} \sin\eta + \eta e^{-\eta} \sin\eta - \frac{21}{8} \right) + \frac{45}{32} \left(1 - \frac{1}{r^2} \right) \right] \cos\theta \sin^2\theta \end{aligned} \tag{9.11}$$

and the corresponding azimuthal vector potential reads (Eq. (9.2))

$$\begin{aligned} \langle \varphi_1 \rangle &= \frac{\langle \psi_1 \rangle}{r \sin\theta} \\ &= \sin(2\theta) \left[\frac{9\sqrt{2}}{8Mr} \left(\frac{1}{8} e^{-2\eta} + \frac{5}{2} e^{-\eta} \cos\eta + \frac{3}{2} e^{-\eta} \sin\eta + \eta e^{-\eta} \sin\eta - \frac{21}{8} \right) + \frac{45}{64} \left(\frac{1}{r} - \frac{1}{r^3} \right) \right] \end{aligned} \tag{9.12}$$

The δ_{DC} predicted by Riley's theory is reflected in main text Fig. 2(d) as well as Fig. 7. We highlight the close agreement in δ_{DC} for higher Womersley numbers $M > 10$. For lower Womersley numbers, Riley's assumption of $M^2 \gg 1$ weakens, which accounts for the quantitative deviation from the present theory with $M < 10$.

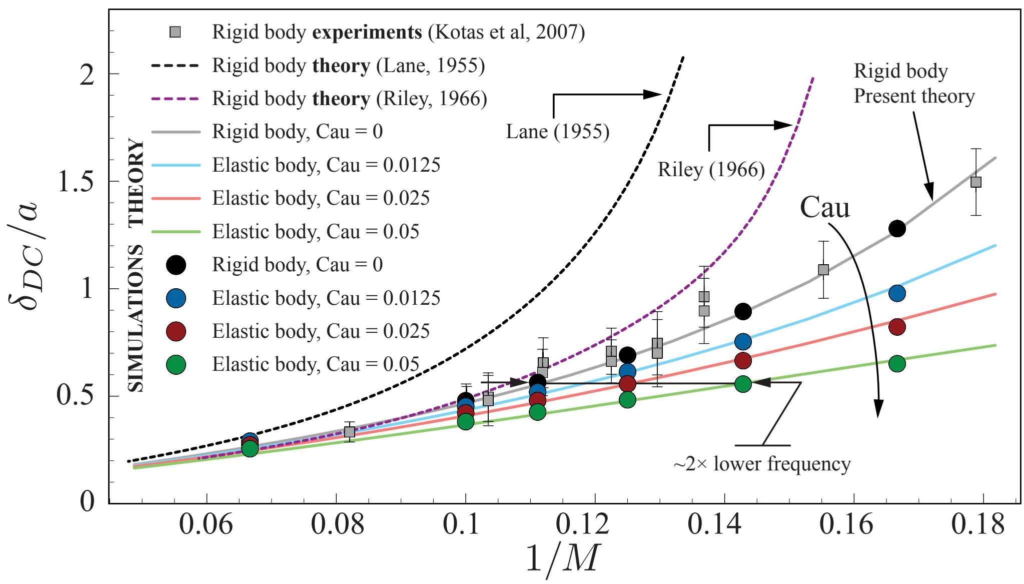

Figure 7: Normalized DC layer thickness (δ_{DC}/a vs. inverse Womersley number ($1/M$) from theory and simulations, for varying body elasticity Cau. An alternative theory (purple dashed line) derived by (Riley 1966), the incomplete theory (black dashed line) of Lane (1955), and experimental results (grey squares) (Kotas *et al.* 2007) in the rigidity limit are plotted for reference.

10. Derivation of the governing equation for visco-hyperelastic solid

Here we outline the derivation for the solid governing equation used in main text Eq. (2.1) and supplementary materials Eq. (1.1).

We start with Cauchy momentum equation

$$\rho \frac{D\boldsymbol{v}}{Dt} = \boldsymbol{\nabla} \cdot \boldsymbol{\sigma} + \rho \boldsymbol{f} \tag{10.1}$$

The body force term $\rho \boldsymbol{f}$ is henceforth dropped as it is absent within our system. In the following steps, we shall replace the Cauchy stress tensor $\boldsymbol{\sigma}$ with an appropriate constitutive relation. To reiterate, in the present work we consider an ***isotropic***, ***incompressible***, *and* ***viscoelastic*** *solid with* ***hyperelasticity***. *We choose a generalized Kelvin-Voigt constitutive model for viscoelasticity (Bulıcek et al. 2012), where we split the Cauchy stress into a fluid-like part and a solid-like part*

$$\boldsymbol{\sigma} = \boldsymbol{\sigma}_f + \boldsymbol{\sigma}_{he} \tag{10.2}$$

For the fluid-like part, we employ the Newtonian viscosity model with Cauchy stress (Panton 2006)

$$\boldsymbol{\sigma}_f = -p_f \boldsymbol{I} + 2\mu_f \boldsymbol{D} \tag{10.3}$$

where $\boldsymbol{D} = D_{ij} = (\partial_j v_i + \partial_i v_j)/2$ is the rate of strain tensor, p_f denotes the pressure, and μ_f is the dynamic viscosity. For the solid-like part, we choose the ***hyperelastic*** *constitutive model as mentioned previously. Given a strain energy density function W, in the incompressibility limit the Cauchy stress may be derived as (Bower 2009)*

$$\boldsymbol{\sigma}_{he} = 2\left[\left(\frac{\partial W}{\partial I_1} + I_1 \frac{\partial W}{\partial I_2}\right)\boldsymbol{B} - \frac{1}{3}\left(I_1 \frac{\partial W}{\partial I_1} + 2I_2 \frac{\partial W}{\partial I_2}\right)\boldsymbol{I} - \frac{\partial W}{\partial I_2}\boldsymbol{B}\cdot\boldsymbol{B}\right] + p_{he}\boldsymbol{I} \tag{10.4}$$

where $\boldsymbol{B} = \boldsymbol{F}\boldsymbol{F}^T$ *is the left Cauchy-Green tensor, with* $I_1 = tr(\boldsymbol{B})$ *and* $I_2 = (I_1^2 - tr(\boldsymbol{B} \cdot \boldsymbol{B}))/2$ *being its first and second tensor invariant. Here* p_{he} *refers is an unknown pressure / hydrostatic stress in the incompressibility limit, analogous to* p_f *in Eq. (10.3). Next, we choose the Neo-Hookean strain energy density function, whose incompressible form reads*

$$W = \frac{G}{2}(I_1 - 3) \tag{10.5}$$

where G *is the shear modulus that is equivalent to Lamé's second parameter* μ*. As an additional note, without the incompressibility condition, one would also expect the third invariant* $I_3 = \det(\boldsymbol{B}) = J^2$ *and the bulk modulus* K *to be relevant, both related to volumetric changes of the material. Substituting the strain energy density function Eq. (10.5) into Eq. (10.4), we obtain the Cauchy stress corresponding to the solid-limit of the viscoelastic material*

$$\boldsymbol{\sigma}_{he} = G\left(\boldsymbol{B} - \frac{1}{3}trace(\boldsymbol{B})\boldsymbol{I}\right) + p_{he}\boldsymbol{I} = G(\boldsymbol{F}\boldsymbol{F}^T)' + p_{he}\boldsymbol{I} \tag{10.6}$$

where $'$ *denotes the deviatoric operator. Substituting the Cauchy stresses Eqs. (10.2), (10.3) and (10.6) into the Cauchy momentum equation Eq. (10.1) and consolidating the unknown pressure terms as* $p = p_f - p_{he}$*, we recover the dimensional form of the solid governing equation*

$$\rho\frac{D\boldsymbol{v}}{Dt} = -\boldsymbol{\nabla}p + \mu_f\boldsymbol{\nabla}^2\boldsymbol{v} + G\boldsymbol{\nabla}\cdot(\boldsymbol{F}\boldsymbol{F}^T)' \tag{10.7}$$

The exact same form of Eq. (10.7) may be found in (Hu et al. *2018), in which the equation is adapted from Upper-Convected Maxwell (UCM) and Oldroyd-B viscoelastic constitutive models. This derivation is also largely identical to the Eulerian governing equations derived by Jain et al (Jain* et al. *2019), although they did not consider visco-elasticity.*

REFERENCES

Angot, Philippe, Bruneau, Charles-Henri & Fabrie, Pierre 1999 A penalization method to take into account obstacles in incompressible viscous flows. *Numerische Mathematik* **81** (4), 497–520.

Bertelsen, A, Svardal, Aslak & Tjøtta, Sigve 1973 Nonlinear streaming effects associated with oscillating cylinders. *Journal of Fluid Mechanics* **59** (3), 493–511.

Bhosale, Yashraj, Parthasarathy, Tejaswin & Gazzola, Mattia 2021*a* A remeshed vortex method for mixed rigid/soft body fluid–structure interaction. *Journal of Computational Physics* **444**, 110577.

Bhosale, Yashraj, Parthasarathy, Tejaswin & Gazzola, Mattia 2022 Soft streaming – flow rectification via elastic boundaries. *Journal of Fluid Mechanics* **945**, R1.

Bhosale, Yashraj, Upadhyay, Gaurav, Cui, Songyuan, Chan, Fan Kiat & Gazzola, Mattia 2023 PyAxisymFlow: an open-source software for resolving flow-structure interaction of 3D axisymmetric mixed soft/rigid bodies in viscous flows.

Bhosale, Yashraj, Vishwanathan, Giridar, Parthasarathy, Tejaswin, Juarez, Gabriel & Gazzola, Mattia 2021*b* Multi-curvature viscous streaming: flow topology and particle manipulation. *arXiv preprint arXiv:2111.07184* .

Bower, Allan F 2009 *Applied mechanics of solids*. CRC press.

Bulicek, M, Málek, J & Rajagopal, KR 2012 On kelvin–voigt model and its generalizations. *Evol. Equ. Control Theory* **1** (1), 17–42.

Gazzola, Mattia, Chatelain, Philippe, Van Rees, Wim M & Koumoutsakos, Petros 2011 Simulations of single and multiple swimmers with non-divergence free deforming geometries. *Journal of Computational Physics* **230** (19), 7093–7114.

Holtsmark, J, Johnsen, I, Sikkeland, To & Skavlem, S 1954 Boundary layer flow near a cylindrical obstacle in an oscillating, incompressible fluid. *The journal of the acoustical society of America* **26** (1), 26–39.

Hu, Xianpeng, Lin, Fang Hua & Liu, Chun 2018 Equations for viscoelastic fluids. In *Handbook* *of mathematical analysis in mechanics of viscous fluids*, pp. 1045–1073. Springer International Publishing.

Jain, Suhas S, Kamrin, Ken & Mani, Ali 2019 A conservative and non-dissipative eulerian formulation for the simulation of soft solids in fluids. *Journal of Computational Physics* **399**, 108922.

Kamrin, Ken & Nave, Jean-Christophe 2009 An eulerian approach to the simulation of deformable solids: Application to finite-strain elasticity. *arXiv preprint arXiv:0901.3799* .

Kamrin, Ken, Rycroft, Chris H & Nave, Jean-Christophe 2012 Reference map technique for finite-strain elasticity and fluid–solid interaction. *Journal of the Mechanics and Physics of Solids* **60** (11), 1952–1969.

Kotas, C.W., Yoda, M. & Rogers, P.H. 2007 Visualization of steady streaming near oscillating spheroids. *Experiments in Fluids* **42** (1), 111–121.

Lane, CA 1955 Acoustical streaming in the vicinity of a sphere. *The Journal of the Acoustical Society of America* **27** (6), 1082–1086.

Liu, Juan, Zheng, Huaiyuan, Poh, Patrina SP, Machens, Hans-Günther & Schilling, Arndt F 2015 Hydrogels for engineering of perfusable vascular networks. *International journal of molecular sciences* **16** (7), 15997–16016.

Longuet-Higgins, Michael S 1998 Viscous streaming from an oscillating spherical bubble. *Proceedings of the Royal Society of London. Series A: Mathematical, Physical and Engineering Sciences* **454** (1970), 725–742.

Lötters, Joost Conrad, Olthuis, Wouter, Veltink, Petrus H & Bergveld, Piet 1997 The mechanical properties of the rubber elastic polymer polydimethylsiloxane for sensor applications. *Journal of micromechanics and microengineering* **7** (3), 145.

Lutz, Barry R, Chen, Jian & Schwartz, Daniel T 2005 Microscopic steady streaming eddies created around short cylinders in a channel: Flow visualization and stokes layer scaling. *Physics of Fluids* **17** (2), 023601.

Lutz, Barry R, Chen, Jian & Schwartz, Daniel T 2006 Hydrodynamic tweezers: 1. noncontact trapping of single cells using steady streaming microeddies. *Analytical chemistry* **78** (15), 5429–5435.

Marmottant, Philippe & Hilgenfeldt, Sascha 2004 A bubble-driven microfluidic transport element for bioengineering. *Proceedings of the National Academy of Sciences* **101** (26), 9523–9527.

Panton, Ronald L 2006 *Incompressible flow*. John Wiley & Sons.

Parthasarathy, Tejaswin, Bhosale, Yashraj & Gazzola, Mattia 2022 Elastic solid dynamics in a coupled oscillatory couette flow system. *Journal of Fluid Mechanics* **946**, A15.

Raney, WP, Corelli, JC & Westervelt, PJ 1954 Acoustical streaming in the vicinity of a cylinder. *The Journal Of The Acoustical Society of America* **26** (6), 1006–1014.

Riley, N 1966 On a sphere oscillating in a viscous fluid. *The Quarterly Journal of Mechanics and Applied Mathematics* **19** (4), 461–472.

Spelman, Tamsin A & Lauga, Eric 2017 Arbitrary axisymmetric steady streaming: Flow, force and propulsion. *Journal of Engineering Mathematics* **105** (1), 31–65.

Vishwanathan, Giridar & Juarez, Gabriel 2019 Steady streaming viscometry of newtonian liquids in microfluidic devices. *Physics of Fluids* **31** (4), 041701.

Wang, Chang-Yi 1965 The flow field induced by an oscillating sphere. *Journal of Sound and Vibration* **2** (3), 257–269.

Wang, Zhixin, Volinsky, Alex A & Gallant, Nathan D 2014 Crosslinking effect on polydimethylsiloxane elastic modulus measured by custom-built compression instrument. *Journal of Applied Polymer Science* **131** (22).